HAL open science

Provenance constraints on the Cretaceous-Paleocene erosional history of the Guiana Shield as determined from the geochemistry of clay-size fraction of sediments from the Arapaima-1 well (Guyana-Suriname basin)

Martin Roddaz, Guillaume Dera, Yannick Mourlot, Gérôme Calvès, Jung-Hyun Kim, Anne-Claire Chaboureau, Stéphanie Mounic, François Raisson

To cite this version:

Martin Roddaz, Guillaume Dera, Yannick Mourlot, Gérôme Calvès, Jung-Hyun Kim, et al.. Provenance constraints on the Cretaceous-Paleocene erosional history of the Guiana Shield as determined from the geochemistry of clay-size fraction of sediments from the Arapaima-1 well (Guyana-Suriname basin). Marine Geology, 2021, 434, pp.106433. 10.1016/j.margeo.2021.106433 . hal-03245370

HAL Id: hal-03245370

https://ut3-toulouseinp.hal.science/hal-03245370

Submitted on 9 Mar 2023

HAL is a multi-disciplinary open access archive for the deposit and dissemination of scientific research documents, whether they are published or not. The documents may come from teaching and research institutions in France or abroad, or from public or private research centers.

L'archive ouverte pluridisciplinaire **HAL**, est destinée au dépôt et à la diffusion de documents scientifiques de niveau recherche, publiés ou non, émanant des établissements d'enseignement et de recherche français ou étrangers, des laboratoires publics ou privés.

Distributed under a Creative Commons Attribution - NonCommercial 4.0 International License

Version of Record: https://www.sciencedirect.com/science/article/pii/S0025322721000153
Manuscript_2e54c4959e4085bb3a58febef18d823b

Provenance constraints on the Cretaceous-Paleocene erosional history of the Guiana Shield as determined from the geochemistry of clay-size fraction of sediments from the Arapaima-1 well (Guyana-Suriname basin)

Martin Roddaz[1*], Guillaume Dera[1], Yannick Mourlot[1], Gérôme Calvès[1], Jung-Hyun Kim[2], Anne-Claire Chaboureau[3], Stéphanie Mounic[1] and François Raisson[3]

[1] Géosciences-Environnement Toulouse, Université de Toulouse; UPS (SVT-OMP); CNRS; IRD; 14 Avenue Édouard Belin, F-31400 Toulouse, France

[2] Korea Polar Research Institute (KOPRI), 26 Songdomirae-ro, Yeonsu-gu, Incheon 21990, South Korea

[3] Total E&P, CSTJF Avenue Larribau, F-64018, Pau Cedex, France

*Corresponding author: Martin Roddaz (martin.roddaz@get.omp.eu)

© 2021 published by Elsevier. This manuscript is made available under the CC BY NC user license
https://creativecommons.org/licenses/by-nc/4.0/

Abstract

Recent studies have emphasized the role of the Equatorial Atlantic Ocean opening on the drainage reorganization and erosion of the West African and northeastern Brazilian cratons during the Cretaceous. However, such studies are lacking regarding the Guiana Shield. To fill this gap, we determined the provenance of sediments deposited in the Suriname-Guyana basin during the Cretaceous-Paleocene based on the total organic carbon (TOC) content, $\delta^{13}C_{TOC}$, major and trace element concentrations, and Sr-Nd isotopic data of nineteen clay-size fraction samples from one industrial well (Arapaima-1). Overall, the absence of correlation between the TOC content, $\delta^{13}C_{TOC}$ and provenance proxies as well as the lack of Ce anomaly indicate that marine authigenesis, reducing conditions, and weathering have not markedly affected the trace element ratios (Eu/Eu*, Cr/Th, Th/Sc) and Sr-Nd isotopic compositions used as provenance proxies. Three samples (Early Cretaceous, Cenomanian and Late Campanian) have radiogenic $\varepsilon_{Nd(0)}$ values >-2.2. The Early Cretaceous sample may have been sourced by Precambrian or Mesozoic mafic rocks of the Guiana Shield or contemporaneous basic volcanic rocks. The Cenomanian sample is likely to have been sourced by basic volcanic rocks of the Caribbean Large Igneous Province or the Takutu rift whereas the Late Campanian sample may have recorded more acid volcanism in the Takutu Rift. The other samples have an overall Guiana cratonic provenance with variable contributions of the Paleoproterozoic and Mesoproterozoic terranes and Jurassic or Precambrian mafic dykes. Increases in $^{87}Sr/^{86}Sr$ ratios and trace element ratios characteristic of more differentiated sources suggest an increasing contribution from the inner part of the Guiana Shield after the Coniacian. Because of the possible presence of active volcanism during the deposition of analyzed samples, post rift mantle upwelling under the

equatorial margin is the favored mechanism to explain the increasing erosion of the Guiana Shield inner parts.

Keywords: Provenance, Cretaceous, Guiana Shield, Guyana-Suriname Basin,

1. Introduction

The structure and geodynamic evolution of transform continental margins have recently received a lot of attention (i.e. Basile, 2015; Mercier de Lépinay et al., 2016; Nemčok et al., 2016). In particular, the conjugate West African, Suriname, Guyana, French Guiana and Brazilian equatorial margins are among the best examples (Basile et al., 2005; Emery et al., 1975; Mascle and Blarez, 1987; Mercier de Lépinay et al., 2016). Whereas the kinematics evolution of the Equatorial Atlantic Ocean and its margins is well constrained in time and space (Heine et al., 2013; Moulin et al., 2010), less attention has been paid to the erosional history of adjacent source areas (i.e., West African and Guiana and Brazilian cratons or Phanerozoic basins). Noticeable exceptions regarding the African margin is the provenance study of Mourlot et al. (2018a) which emphasized that the West African Craton (WAC) may be viewed as a dynamic area during the Cretaceous opening of the Equatorial Atlantic Ocean. Using the Nd isotopic composition of marine sedimentary rocks sampled offshore along the African margin, these authors have highlighted that the erosion the WAC evolved from its outer parts in the Albian−Middle Cenomanian interval to its inner parts in the Campanian−Maastrichtian (Mourlot et al., 2018a).

Like other Atlantic passive margins, the Brazilian and Guyana-Suriname margins are bordered by elevated low relief inland plateaus separated from a a higher relief coastal plain by one or more steep escarpments (Cogné et al., 2012; Gallagher et al., 1994; Gallagher and Brown, 1999; Hiruma et al., 2010; Japsen et al., 2012; Jelinek et al., 2014; Tello Saenz et al., 2003). The presence of a Late Cretaceous “peneplanation surface” in the inner part of the Guiana Shield cropping out at elevation > 900 m asl is ascribed to Campanian erosion that may have affected this part of the Guiana Shield (Sapin et al., 2016). In northeastern Brazil, various

thermochronological and geomorphological studies have presented evidences of Late Cretaceous uplift (Harman et al., 1998; Morais Neto et al., 2009; Peulvast and Bétard, 2015; Potter, 1997). However, all these studies are based on mapping or sampling of isolated Cretaceous outcrops and this may question the representativeness of these studies at basin scale. To date there is no provenance study dealing with the Cretaceous erosional history of the Guiana Shield.

Determining the provenance of well dated deep-sea sediments deposited in marginal basins may be particularly useful to provide constraint on the erosional history of cratons (Clift and Blusztajn, 2005; Mourlot et al., 2018a). Many tools exist to determine the provenance of sedimentary rocks including sandstone petrography, clay mineralogy, heavy mineral analyses, geochronological dating on accessory minerals, major and trace element geochemistry and Sr-Sm-Nd isotopic compositions of bulk sedimentary rocks (see for instance Basu et al., 1990; Caracciolo, 2020; Cullers, 2000; Dickinson, 1985; Dickinson and Suczek, 1979; Garzanti, 2016, 2019; Garzanti and Andò, 2019; McLennan et al., 1993a; Weltje, 2012 and references therein). All of these tools are subjected to biases related to source-rock mineral fertility (see for instance Chew et al., 2020; Dickinson, 2008; Malusà et al., 2016, 2013), pre and post depositional processes including weathering, grain-size sorting and diagenesis (see for instance (Bouchez et al., 2011; Fedo et al., 1995; Garzanti et al., 2008, 2009, 2014; Lawrence et al., 2011; McLennan et al., 1993a; Moquet et al., 2020; Nesbitt et al., 1996; Roddaz et al., 2006, 2014; Rousseau et al., 2019; Viers et al., 2008) and analytical procedures (Andersen et al., 2019; Chew et al., 2020; Malusà et al., 2013; Vermeesch, 2018, 2004). In addition, the low amount of material available for well or core sample makes geochronological dating methods (especially U-Pb dating on zircon) difficult to use. Trace elements ratios (i.e. Th/Sc, Cr/Th, Eu/Eu*) as well as Sr-Nd isotopic composition of clay size sediments may be preferred to establish a complete integration

of drainage pathways from the most distant cratonic areas to oceanic basins (Patchett et al., 1999) because they are not biased by grain-size sorting (e.g. Cullers, 2000; McLennan et al., 1993) and require a lower amount of bulk sediment (~3 g, Bayon et al., 2002) These geochemical approaches have been recently used to determine the source of the Late Eocene to Quaternary sediments deposited in the Mozambique Channel (Roddaz et al., 2020) or to reconstruct the Cretaceous erosional history of the WAC (Mourlot et al., 2018). Furthermore, the Nd isotopic composition of past sediments deposited in ocean margins can provide constraints for determining the influence of continental Nd inputs released from river-borne lithogenic sediments deposited at ocean margins on Nd isotopic composition of past oceans. Indeed, Rare Earth Elements (REE) release from lithogenic sediments in river discharge may ultimately dominate all other REE inputs to the oceans (Jeandel et al., 2007; Jeandel and Oelkers, 2015; Rousseau et al., 2015). Such constraints are crucial for all oceanic circulation reconstruction based on the Nd composition of past oceanic masses (e.g. (Dera et al., 2015; Donnadieu et al., 2016; Mourlot et al., 2018b). Currently, the only Nd isotopic data available for the Cretaceous sediments of the Guyana and Brazilian margins of the Equatorial Atlantic Ocean are those from Martin et al. (2012). These data were obtained on fish teeth and sediments from the Demerara Rise (ODP Leg 207) which was a bathymetric high during the Cretaceous (e.g. Arthur and Natland, 1979. Loncke et al., 2019) and may have been potentially more influenced by oceanic currents than other parts of the equatorial margin basins.

The aim of this study is to determine the provenance of siliciclastic sediments deposited at the Suriname-Guyana basin during the Early Cretaceous-Paleocene based on TOC content, $\delta^{13}C_{TOC}$, major and trace element concentrations and Sr-Nd isotopic data of nineteen clay-size fraction of sediment samples from one industrial well Arapaima-1 (AR-1, Fig. 1). Determining

the provenance of these sediments may help to bridge the gap between provenance studies regarding West African and Guiana cratons and may provide constraints on the erosional history of the Guiana craton.

2. Geological setting and sedimentary sources

2.1 Tectonic and geodynamic setting

The Guyana-Suriname basin is located along the passive margin of northeastern South America (Fig. 1). It includes the offshore of Guyana, Suriname and French Guiana. It is delimited by the Demerara Plateau to the east, the Barbados Ridge accretionary prism to the west, the Guiana shield to the south and the Demerara Abyssal plain to the north (Fig. 1). The tectonic evolution of the Guyana-Suriname basin can be divided into three main geodynamic periods linked to the opening of the Atlantic Ocean from the Early Jurassic (~200 Ma) to present (Yang and Escalona, 2011). The first geodynamic period is related to the Jurassic rifting between South America and North America. It was first initiated in the Central Atlantic region and resulted in east-west extension with a large component of dextral shearing in the Guyana-Suriname basin (Gouyet et al., 1994). This rifting period resulted in the formation of grabens in the present-day offshore region of the Guyana-Suriname basin and in the east-west–oriented Takutu graben separating the Guyana shield in two parts (Fig. 1). The thick (approximately 21 km) volcanic basement of the Demerara Rise formed as a result of syn-rift-related volcanism linked to the Bahamas hot spot at the initial opening of the Central Atlantic (Basile et al., 2020; Reuber et al., 2016). This volcanism produced a marine substrate upon which the Late Jurassic-Early Cretaceous carbonate section of the Demerara rise developed (Basile et al., 2020; Reuber et al., 2016).

During the Early Cretaceous, Southern Africa and South America started to split off because of the counterclockwise rotation of Africa relative to South America (Mann et al., 1995; Pindell, 1991), resulting in two conjugate margins: the Guinea Rise on the African margin and the Demerara Rise on the South American margin. The drift stage of continental separation started to develop in the southernmost part of the South Atlantic Ocean at around 135 Ma (Late Valanginian–Early Hauterivian) (Hall et al., 2018) and then propagated northward toward the Equatorial Atlantic Ocean. This latter propagation of the South Atlantic rifting resulted in the formation of an erosional unconformity affecting the Guyana-Suriname basin and was responsible for the sedimentary hiatus between the upper Aptian and the lower Albian (Yang and Escalona, 2011). The pre-Albian section of the Demerara Rise was inverted and cut by a peneplanation surface with a strong angular unconformity prior to the Early Cretaceous opening of the Equatorial Atlantic seaway (Reuber et al., 2016).

The Equatorial Atlantic Ocean opened East of the Demerara Plateau during the Late Albian (see Moulin et al., 2010 and references therein). A kinematic change at 105 Ma (Albian) associated to the northward displacement of the triple junction between Africa, North America and South America plates (Müller and Smith, 1993) induced the formation of numerous E–W fracture zones North of the Demerara Plateau (Basile et al., 2013). Between the Albian and the Eocene, drifting between Africa and South America induced a general collapse of the unstable shelf edge and is responsible for the main extensional regime in the Guyana-Suriname basin (Yang and Escalona, 2011). This predominantly transcurrent setting may have favored the formation of a large pull-apart basin with a gentle thermal subsidence similar to the conjugated Guinean continental margin (Benkhelil et al., 1995).

2.2 Stratigraphy

2.2.1 Stratigraphy of the Guyana-Suriname basin

The sedimentary infilling of the Guyana-Suriname basin may be divided into four stratigraphic sequences that overlay the Jurassic basement. These sequences are termed as follows: S1 (Cretaceous), S2 (Paleogene), S3 (Early-Middle Miocene), S4 (Late Miocene to Pliocene) (Yang and Escalona, 2011). Details on the stratigraphy of the S1 sequence and associated references can be found in Yang and Escalona (2011). The S1 sequence starts with the Barremian basal clastic sandstones of the Stabroek Formation overlaid by the nonmarine siliciclastic deposits of the Potoco Formation. These formations are separated from the Albian to Turonian shelf marine platform deposits belonging to the Canje Formation by a Late Aptian–Early Albian(?) regional unconformity. The Canje Formation is composed of black shales with average total organic contents (TOC) between 4 and 7%, and reaching 29% in the Demerara Rise in the DSDP Site 1259 (Meyers et al., 2006). These formations are then overlaid by the New Amsterdam Formation, a siliciclastic interval interpreted as a coastal environment with sand and lagoonal deposits (Lawrence and Coster, 1985). This formation corresponds to reservoirs in the Arapaima-1 well in offshore Guyana (Yang and Escalona, 2011). The top of the Mesozoic is marked by an erosional unconformity overlaid by Paleocene to Eocene carbonate shelf deposits of the George Town Formation (Yang and Escalona, 2011).

2.2.2 Stratigraphy of the Arapaima-1 well

The stratigraphy and sedimentology of Cretaceous sequences of the Arapaima-1 well were reinterpreted by the TOTAL department of stratigraphy (Mourlot, 2018) and are presented in Fig. 2. The Early Cretaceous (pre-Aptian) is characterized by medium to coarse grained

sandstones with common shale and limestone intervals deposited in inner to outer shelf paleoenvironments. These clastic deposits are then separated from Late Albian shelf limestones by an erosional unconformity. These Late Albian shelf limestone are then overlaid by the first sequence of green to grey shales slightly enriched in TOC (1% wt) associated with a lowering of the sedimentation rate (Mourlot, 2018). This sequence is gradually overlain by Cenomanian deposits characterized by alternation of shales and sandstones. A two fold increase in sedimentation rate is noted for the Cenomanian clastic deposits when compared with older Early Cretaceous sediments (Mourlot, 2018). This Cenomanian clastic sequence is then followed by Cenomanian middle to outer shelf limestone deposits. The uppermost Cenomanian to Coniacian deposits consist in dark-grey to brown shales interbedded with siltstone and very fine sandstone and are characterized by an increase of organic-content (from 2% wt up to 4% wt, Fig. 2). This sequence can be correlated with the Canje Formation which is also composed of organic rich shales with average TOC between 4 and 7%. During the same period, the Demerara plateau also record an enrichment in Total Organic Carbon, with the TOC concentration reaching up to 29% at DSDP Site 1259 (Meyers et al., 2006). The Santonian to Paleocene sediments are characterized by alternation between medium to coarse sandstones and mainly non organic rich shales. The sedimentation rate is much higher during the Santonian, respectively six fold and three fold than the Early Cretaceous–Late Albian and Cenomanian–Coniacian intervals (Mourlot, 2018).

2.3. Sedimentary sources

The potential sources of the studied sediments include the Guiana Shield, the proto Andes, and the Caribbean Large Igneous Province magmatic rocks. Additionally, Aptian-Albian volcanism encountered on the Guinea Plateau (Olyphant et al., 2017) may be a potential source.

The Albian volcaniclastic units were dated at *ca* 106 Ma (Olyphant et al., 2017) and related to the silica under-saturated alkaline-nepheline-syenite suite of the Los Archipelago ring structure dated at ca 104.3 ± 1.7 Ma and located off the south-western shore of Conakry, Guinea (Moreau et al., 1996) . The Guiana Shield is mainly composed by Paleoproterozoic magmatic and metamorphic rocks accreted to two Archean nuclei during the main or late phase of the Trans-Amazonian orogeny (i.e., the Imataca block to the northwest and the Amapá block to the southeast; AAIG in Fig.3) (Delor et al. 2003; da Rosa-Costa et al., 2006; Gaudette et al., 1996, 1978; McReath and Faraco, 2005; Vanderhaeghe et al., 1998). Based on geochronological and structural data, the Guiana shield may be divided into six main provinces decreasing in age southwestward from 2.5 to 1.2 Ga: Amazônia Central, Maroni-Itacaiúnas, Tapajós-Ventuari, Rio Negro-Juruena, Rondônia-San Ignacio, and Sunsás (Santos et al., 2000; Teixeira et al., 1989; Cordani et al. 2000). From a lithological point of view, the northernmost part of the shield is occupied by an extended greenstone belt (GB) amalgamated with Paleoproterozoic granitoids, gneiss, and felsic (meta)volcanic series (PGGF) (Barreto et al., 2013; Gruau et al., 1985), and bounded to the south by a high-grade granulite belt (PHGB) (Klaver et al., 2015; de Roever et al. 2003). Overall, the rest of the shield is dominated by younger Paleoproterozoic PGGF marked by intrusions of Mesoproterozoic granite plutons (MG) in the Rio Negro province (Tassinari 1981; Sato 1998; Heinonen et al., 2012). Paleoproterozoic sediments related to the erosion of the Trans-Amazonian orogen are also present in the northwest part of the shield and consist in 3000 m thick alternations of sandstones, conglomerates and pyroclastic rocks (PRS) belonging to the Roraima Formation (Priem et al., 1973). All the units cited above are intruded by sparse Paleoproterozoic mafic intrusions (PMI) (i.e., Avanavero dolerites, (Hebeda et al., 1973; Reis et

al., 2013) as well as Jurassic mafic dykes and sills (JMD) related to the Central Atlantic Magmatic Province (CAMP) activity at 200 Ma (De Min et al. 2003; Deckart et al., 2005).

As mentioned above, a rifting affected the Guiana shield from the Jurassic to Cretaceous, resulting in the formation of grabens stretching from SW Guyana to northern Brazil and constituting the Takutu basin. Upstream of the paleo-Berbice delta (Erlich and Keens-Dumas 2007), this narrow intracratonic basin is especially important as it could represent the main pathway of the Berbice paleodrainage network during the Cretaceous (Figs. 1 and 3) (Lujan and Armbruster, 2011). The infilling of the basin consists first of the 900-1700 m thick tholeiitic basalts of the poorly dated Apoteri volcanic Formation (Crawford et al., 1985). A Jurassic age is commonly ascribed to these basaltic rocks (Berrangé and Dearnley, 1975; Crawford et al., 1985; Yang and Escalona, 2011), in association to the volcanic events of the Central Atlantic Magmatic Province (CAMP) with peak activity at 200 Ma (Marzoli et al., 1999). However, two K/Ar radiometric dating on basaltic lava flows yield Early Cretaceous ages at 114 ± 3 Ma and 116 ± 4 Ma (Berrangé and Dearnley, 1975) so that the Apoteri volcanic Formation might be younger than previously thought. Overlying the Apoteri volcanic Formation are the poorly dated shales and halites of the Manari and Pirara formations followed by the 1600 cm to 3500 m thick Jurassic to Cretaceous shales, sandstone, siltstones, and micritic limestones of the Takutu Formation (Crawford et al., 1985). This formation developed in fluvial and coastal settings. Pyroclastic flows, up to 87% in SiO_2 content, are recorded in the upper part of the Takutu Formation (Crawford et al., 1985).

All the geological units of the Guiana Shield defined above present different ages and lithologies (mafic vs. felsic) making them suitable to distinguish in term of major and trace elemental compositions but also $^{87}Sr/^{86}Sr$ and εNd(0) values. To better characterize the sources

of studied Cretaceous-Paleocene sediments, we compiled 568 published Sr and Nd isotope values measured on magmatic and metamorphic rocks representative of six characteristic end-members of the Guiana shield (Table 1 and supporting information Table S1 for details and references). By increasing $\varepsilon Nd_{(0)}$ value, these latter include the Archean granitoids (AAIG) with median $\varepsilon Nd_{(0}$and $^{87}Sr/^{86}Sr$ values at -31.4 (standard deviation (S.D.): 9.3, Table 1) and 0.79509 (S.D.: 0.335623, Table 1), the Paleoproterozoic granitoids and felsic series (PGGF) at -23.4 (S.D.: 8.0, Table 1) and 0.77395 (S.D.: 0.4638016, Table 1) the Paleoproterozoic high-grade belt (PHGB) at -21.2 (S.D.: 6.2, Table 1) and 0.72025 (S.D.: 0.1571444, Table 1), the Mesoproterozoic granitoids (MG) at -18.5 (S.D.: 2.1, Table 1) and 0.77460 (S.D.: 0.05247612, Table 1), the Paleoproterozoic mafic intrusions and greenstone belt (PMI-GB) at -8.9 (S.D.: 7.1, Table 1) and 0.71051 (S.D.: 0.006878231, Table 1), and the Jurassic mafic dykes (JMD) at -0.2 (S.D.: 3.1, Table 1) and 0.70647 (S.D.: 0. 0.001692758, Table 1 and Fig. 3). For comparison, this database was completed by 47 $^{87}Sr/^{86}Sr$ and ε $Nd_{(0)}$ values of later Cretaceous to modern sediments deposited in the Demerara abyssal plain and Demerara Rise (Martin et al., 2012; Schulte et al., 2009; White et al., 1985), as well as 110 Sr-Nd isotopic compositions of suspended particulate matter and dissolved Sr transported by the main tropical rivers of the northeastern part of South America (i.e., Amazon, lower and upper Orinoco, Rio Negro, Maroni, Trombetas, Caroni) (Allègre et al., 1996; Goldstein et al., 1997; Palmer and Edmond, 1992; Rousseau et al., 2019; Santos et al., 2015).

3. Materials and Methods

3.1 Sampling

Nineteen Early Cretaceous to Paleocene fine-grained sedimentary rocks were sampled from the Arapaima-1 exploration well (Fig. 1). These fine-grained sedimentary rocks were deposited in shallow marine mixed clastic and carbonates depositional environments. There is uncertainty regarding the limits between the Late Albian and the Cenomanian and between the Santonian and the Late Campanian in the well due to lack of biostratigraphic data. Otherwise, the time resolution of samples is at the sub-stage level (*i.e.*, ~2 to 3 Ma). These samples provide sufficient time resolution to identify long-term trends in sedimentary provenance.

3.2 Bulk organic geochemical analysis

The TOC content of sediments and its stable carbon isotopic compositions ($\delta^{13}C_{TOC}$) were analysed at the University of Hanyang (South Korea). Precisely weighed aliquots (0.5-16 g) of crushed and homogenized samples were decalcified by adding about 8 mL of 1M HCl. After shaking overnight (~12 h) to remove carbonates prior to analysis, the TOC content and $\delta^{13}C_{TOC}$ values were determined by EA-IRMS (elemental analyzer-isotope ratio mass spectrometry, EuroEA-Isoprime IRMS, GV instruments, UK). The TOC content and isotope values were calibrated against a standard (IAEA-CH-6, TOC = 42.1 %, $\delta^{13}C$ = -10.44 ‰). The analyses were performed at least in duplicate. The TOC data are given in weight percentage (wt%) and the $\delta^{13}C_{TOC}$ values are reported in the standard delta notation relative to the Vienna Pee Dee Belemnite (VPDB) standard. The analytical precision (as standard deviation for repeated measurements of the internal standard IAEA-CH-6, *n=18*) is 1.1 wt% for TOC and 0.2 ‰ for $\delta^{13}C_{TOC}$.

3.3 Major and trace elements and Sr-Nd isotopes

3.3.1 Sample preparation

Each sample was finely crushed in an agate mortar. About 3 g of the crushed sediment were placed into 50 ml centrifuge tubes for sequential leaching to remove the non-terrigenous sedimentary components following the method of Bayon et al. (2002). Three different solutions composed of 5% acetic acid, 15% acetic acid and hydroxylamine hydrochloride (0.05 M) and hydrogen peroxide (H_2O_2, 5%) were then added to remove the carbonates, Fe-Mn oxides and organic carbon, respectively. After the removal of non-terrigenous components, the residual fractions were cleaned with ultrapure water (MQ-H_2O, 18 MΩ). Clayey (<2 μm) and silty (2-63 μm) fractions were then separated by centrifugation in two steps. First, 25 ml of MQ-H_2O were added to the detrital residues in the tubes, shaken vigorously, and then centrifuged for 2 min at 1000 rpm (133 g). The clay-rich supernatants were immediately transferred into new 50 ml centrifuge tubes. Another 25 ml of MQ-H_2O was added to silt-rich detrital residues, mixed thoroughly again, centrifuged for 2.5 min at 800 rpm (85 g), and transferred into corresponding centrifuge tubes. Finally, clay-size fractions were collected after decantation (48 hours) and centrifugation at 3500 rpm (1630 g) (Bayon et al., 2015). These clay-size fractions were then analyzed for their major and trace element concentrations and their Sr-Nd isotopic compositions.

3.3.2 Major and trace element analyses

The major and trace element concentrations were measured at the Service d'Analyse des Roches et Minéraux (SARM, INSU facility, Vandoeuvre-Les-Nancy, France) by ICP-OES (Na, Mg, K, Ca, Sc, Ti, Mn, Fe, Al, Si and P) and ICP-MS (Rb, Cs, Ba, Sr, Th, U, Y, Zr, Nb, Hf, Cr, V, Co, Cu, Ni, Zn, La, Ce, Pr, Nd, Sm, Eu, Gd, Tb, Dy, Ho, Er, Tm, Yb, Lu and Ta) after alkali

fusion. Analytical details are available on http://helium.crpg.cnrs-nancy.fr/SARM/ and in Carignan et al. (2001). Uncertainty is lower than 5% for elements measured by ICP-OES, and lower than 10% for elements measured by ICP-MS (see supplementary material Table S2).

3.3.3 Nd-Sr isotopes compositions

The Nd-Sr isotopic compositions were measured at Géosciences Environnement Toulouse (GET) in France. About 100 mg of the leached detrital residue fractions were accurately weighed in cleaned Savillex PFA vials and then digested by several hot acid attacks. The analyzed fractions were firstly digested in hydrogen peroxide for 24 hours at ambient temperature, and then digested in HNO_3 for 24 hours at 80°C followed by HF-HNO_3 for 24 hours at 80°C, and, finally HCl+HNO_3 for 24 hours at 115°C. Blank tests were performed to estimate the level of contamination induced by the acid digestion, but it was found to be negligible. Aliquots containing about 1000 ng of Sr and Nd were loaded into the ion exchange columns. Strontium and Nd were separated using the Sr-SPEC, TRU-SPEC and LN-SPEC resins (Eichrom). The isotopic values of both elements were measured using a Finnigan Mat 261 thermal ionization mass spectrometer and a Triton Thermal Ionization Mass Spectrometer in dynamic mode during the same runs as performed for clay-size sediments of the DSDP 25 Site 242 analyzed in (Roddaz et al., 2020). During the Nd runs, a $^{146}Nd/^{144}Nd$ ratio of 0.7219 was used to correct the signal for mass fractionation. For each sample, checks were made for the absence of Samarium (Sm). The accuracy of the measurements was estimated on the La Jolla standard. Repeated analyses of the La Jolla standard gave a $^{143}Nd/^{144}Nd$ ratio of 0.511867 ± 0.000018 (2 S.D, n = 12) in agreement with the recommended value of 0.511858 (Lugmair et al., 1983). During the Sr runs, $^{86}Sr/^{88}Sr$ = 0.1194 was used to correct the signal for mass fractionation. The accuracy of the $^{87}Sr/^{86}Sr$ measurements was checked against the NBS 987 standard (= 0.710240) Hodell et al.,

2007). Repeated analyses of the NBS 987 standard gave an $^{87}Sr/^{86}Sr$ ratio of 0.710231 ± 0.000032 (2SD, n = 15) in agreement with the recommended value of Hodell et al. (2007) therefore no instrumental bias needs to be taken into account. Total blanks (acid digestion plus column chemistry) for Nd and Sr were checked by ICP-MS and found to be negligible (<1 per mil) compared to the Nd and Sr amounts loaded onto the columns**.**

The measured $^{143}Nd/^{144}Nd_{sample}$ ratios are expressed in epsilon notation as the fractional deviation in parts per 10^4 (units) from $^{143}Nd/^{144}Nd$ value of the Chondritic Uniform Reservoir (CHUR). This notation is defined as:

$$\varepsilon_{Nd(t)} = [(^{143}Nd/^{144}Nd)_{sample(t)} / (^{143}Nd/^{144}Nd)_{CHUR(t)} - 1] \times 10^4$$

where t indicates the time at which ε_{Nd} is calculated. Here, no time correction is applied (t = 0) and the $^{143}Nd/^{144}Nd_{CHUR(0)}$ = 0.512638 (Jacobsen and Wasserburg, 1980).

4. Results

4.1 Organic geochemistry and $\delta^{13}C_{TOC}$ data

The TOC results for the Arapaima-1 well are variable with values ranging from 0.2 to 4.6 wt% through the studied interval (Table 2). The Cenomanian to Santonian sedimentary rocks (AR1-11B to AR1-17B samples) appear to be more enriched in organic matter (TOC>2%) compared with other sedimentary rocks (Table 2 and Fig. 2). The $\delta^{13}C_{TOC}$ of analyzed samples range between -28.4 (Cenomanian, samples AR1-11E and AR1-11F) and -25.0 (Early Turonian, sample AR1- 12A, Table 2). Compared with compilations of long-term Cretaceous trends in NW Tethyan and Pacific $\delta^{13}C_{bulk}$ data (Bodin et al., 2015; Friedrich et al., 2012), our data show

similar sharp positive isotopic excursions in the Cenomanian (between samples AR1-9 and AR1-10, Table 2) and at the Cenomanian-Turonian boundary (samples AR1-11E and AR1-11F, Table 2). However, the younger $\delta^{13}C_{TOC}$ data do not fit the long-term Cretaceous evolution of $\delta^{13}C_{bulk}$ data recorded in the NW Tethyan and Pacific (Friedrich et al. 2012).

4.2 Major elements, Large-Ion Lithophile Elements (LILE), High Field Strength Elements (HFSE) and Trace Transition Elements (TTE)

Figure 4 shows the elemental concentrations of major elements, LILE, HFSE and TTE of samples normalized to the Post Archean Australian Shales (PAAS) concentration (Pourmand et al., 2012; Taylor and McLennan, 1985). As a whole, the elemental composition of the analyzed sample is rather uniform. They are all depleted in MnO, CaO, K_2O, Rb, Cs, Sr, Th, Y, Zr, Nb, Hf et Co against PAAS (Table 3 and Fig. 4). With the exception of two Early Cretaceous samples (AR1-1 and AR1-7) and Santonian- Paleocene samples (AR1-21, AR1-23, AR1-24), they are enriched in Cr and V with respect to PAAS (Table 3 and Fig. 4). However, the analyzed samples are more contrasted regarding their concentrations in Na_2O, P_2O_5, Ba and U against PAAS. Overall, Santonian-Paleocene sediments are less concentrated in major and trace elements when compared with older sediments. But, no apparent trend of major depletion or enrichment in elemental concentration is recorded with the age of sediments.

It is possible to assess the degree of source-area weathering and the paleoweathering conditions of ancient sediments using the Chemical Index of Alteration (CIA) (Fedo et al., 1995; Nesbitt and Young, 1982). This index measures the weathering intensity of feldspars relative to unaltered protoliths, and is defined as: $CIA = [Al_2O_3/(Al_2O_3+CaO^*+Na_2O+K_2O)]\times100$ (in molar proportions), where CaO* represents the CaO content in the silicate fraction. CIA values for unaltered plagioclase and K-feldspars typical of unaltered upper crustal rocks are approximately

equal to 50, whereas higher CIA values represent higher degrees of weathering. For comparison, the CIA value of the PAAS standard, which is representative of the upper continental crust composition, is equal to 67 (Taylor and McLennan, 1985).

Here, the CIA values of analyzed samples range from 61 to 89 and are therefore higher than those of the PAAS, except for one sample (AR1-7, CIA~61). Overall, and with the exception of the Coniacian sample AR1-17A (CIA~74), the Early Cretaceous samples (AR1-1, AR1-6, AR1-7) and Cenomanian samples (AR1-9 to AR1-11F) have lower CIA values (70-78, Table3) than younger Turonian to late Campanian samples (CIA ≥ 80, Table 3).

Early Cretaceous to Early Santonian samples have Cr/Th ratios higher than PAAS (37.9-10.2, Table 3) whereas younger samples have Cr/Th ratios lower than PAAS. Analyzed samples have Th/Sc ratios ranging between 0.27 and 1.12 (Table 3). With the exception of two Cenomanian samples (AR1-11E and AR1-11F), the Th/Sc ratios is increasing as the age of the samples is becoming younger (Table 3).

4.3 Rare Earth Elements (REE)

To facilitate comparisons with sediments derived from basic or felsic sources (Cullers, 2000) and the PAAS (Pourmand et al., 2012; Taylor and McLennan, 1985), the Eu anomaly is calculated with respect to chondrites: $Eu/Eu^* = Eu_N/(Sm_N \times Gd_N)^{1/2}$ where $_N$ refers to the chondrite-normalized concentration value (Condie, 1993). The Cerium anomaly (ΩCe) normalized to PAAS is calculated following (De Baar et al., 1985) : $\Omega Ce = 2 \times (Ce_{sample}/Ce_{PAAS}) / [(La_{sample}/La_{PAAS}) + (Pr_{sample}/Pr_{PAAS})]$, where X_{sample} is the concentration of samples and X_{PAAS} refers to the concentrations of the PAAS standard.

When normalized against PAAS, most of the analyzed samples have flat REE patterns and variable Eu anomalies (Fig. 5). The Santonian to Paleocene samples are more enriched in Light REE (LREE) and in Middle REE (MREE) than PAAS (Fig. 5). Three Cenomanian samples (AR1-11B, AR1-11D, AR1-11E) show enrichment in Heavy REE (HREE) against LREE and MREE (Fig. 5 and Table 3). The analyzed sample Ce anomalies display a narrow range of values (0.85-1.01) close to that of the PAAS standard (*i.e.*, ΩCe = 1). The analyzed values are systematically higher than those measured in authigenic smectites and seawater (ΩCe <0.50, De Baar et al., 1985) and they do not show any variation with stratigraphic position. The Eu/Eu* ratios of the analyzed samples range between 1.26 and 0.67 and are higher compared to the PAAS standard (*i.e.*, Eu/Eu* = 0.58). With the exception of one Cenomanian sample (AR1-10), there is an overall increase of the Eu anomaly (i.e decrease of the Eu/Eu* ratio) with the age of the sample (Figs 5 and 6 and Table 3).

4.4 Sr-Nd isotopes

The $^{87}Sr/^{86}Sr$ isotopic composition of the samples range from 0.714598 to 0.773011 while their $\varepsilon_{Nd(0)}$ values range from -0.6 to -21.2 (Table 4). Median values for $^{87}Sr/^{86}Sr$ isotopic compositions and $\varepsilon_{Nd(0)}$ values are 0.736 and -18.8 respectively. There is no correlation between the Sr and Nd isotopic composition of analyzed samples (see Table S3 in supplementary dataset). Overall, the $^{87}Sr/^{86}Sr$ ratios of Arapaima-1 well samples can be split into three groups. Samples AR1-1 (Early Cretaceous) to AR1-9 (Cenomanian) and Coniacian samples (AR1-17A and AR1-17B) have quite similar low radiogenic $^{87}Sr/^{86}Sr$ ratios ranging between 0.721 and 0.733 (Table 4). The other Cenomanian and the Turonian samples show strong variation in their $^{87}Sr/^{86}Sr$ ratios (0.715-0.761). And overall, if we except the Early Turonian sample (AR1-12A), the youngest late Santonian to Paleocene analyzed samples have the more radiogenic $^{87}Sr/^{86}Sr$ ratios

of the analyzed samples (0.749-0.775, Table 4 and Fig. 6). Most of the analyzed samples have low radiogenic Nd isotope composition with $\varepsilon_{Nd(0)}$ values generally between -15.8 and -21.2 (Table 4). Only three samples (Early Cretaceous AR1-1, Cenomanian AR1-11D and Late Campanian AR1-23) have high radiogenic signatures with $\varepsilon_{Nd(0)}$ values between -2.2 and -0.6 (Table 4). Two samples (Cenomanian AR11E and Santonian? AR1-21) have intermediate Nd isotopic composition with $\varepsilon_{Nd(0)}$ values of -12.2 and -13.6 respectively (Table 4).

5. Discussion

5.1. Influence of weathering, authigenesis and anoxic conditions on provenance proxies

The REE content, Eu anomalies, elemental ratios (Cr/Th and Th/Sc) and Sr-Nd isotopic compositions of sedimentary rocks may be used as robust tools for determining the provenance of marine sediments (McLennan et al., 1993), to the condition that they are not affected by weathering and syndepositional clay authigenesis. For instance, high Eu anomalies and Th/Sc and low Cr/Th are characteristic of felsic and more highly differentiated source rocks, whereas high Cr/Th and low Eu anomalies and Th/Sc suggest more mafic and less differentiated source rocks (Cullers, 2000; McLennan et al., 1993b). In general, these ratios as well as the REE content are not significantly affected by diagenesis or weathering (Cullers, 2000; Fedo et al., 1995; McLennan, 1989; McLennan et al., 1993a) The absence of any correlation (see Table S3 in supplementary dataset) of CIA and Al/Si with REE content, Eu/Eu*, Cr/Th, Th/Sc, $^{87}Sr/^{86}Sr$ isotopic compositions and $\varepsilon_{Nd(0)}$ suggests that chemical weathering has not modified these provenance proxies. Regarding authigenesis effects, any influence from carbonates, Fe-Mn oxides or organic matter formed under marine conditions should have been removed by the sequential carbonate dissolution and leaching steps. In addition, there is no correlation between

TOC content and $\delta^{13}C_{TOC}$ and provenance proxies (Eu/Eu*, Cr/Th, Th/Sc, $^{87}Sr/^{86}Sr$ isotopic compositions and $\varepsilon_{Nd(0)}$) suggesting that enrichment and preservation of organic matter are not affecting these proxies. Moreover, the REE patterns of authigenic smectites formed in deep-water environments are characterized by LREE depletion, HREE enrichment and strong negative Ce anomalies (ΩCe < 0.50, De Baar et al., 1985) typical of seawater (Piper, 1974). Here, most of the analyzed samples have Ce anomalies higher than or equal to 0.85, with flat REE patterns against PAAS corresponding to the "shales" field in Fig. 7. Only three Cenomanian samples (AR1-11B, AR1-11D, AR1-11E) show enrichment in HREE over LREE and plot between the "shales" and "seawater" fields in Fig. 7. However, as they have low Ce anomalies against PAAS (ΩCe between 0.88 and 0.92), this suggests that, even if authigenic smectites might have been incorporated during early diagenetic processes, its proportion was much less than the detrital fraction. Finally, it is worth noting that diagenetic remobilization of Eu under reducing conditions might lead to the development of high positive Eu anomalies (MacRae et al., 1992). As anoxic to suboxic conditions are suggested from geochemical and sedimentological proxies onto the Demerara Rise (i.e., Ocean Drilling Program Leg 207 Site) in the Cenomanian-Turonian interval (Berrocoso et al., 2008; Hetzel et al., 2009), this process could explain the high Eu/Eu* value (1.26) of the Cenomanian sample AR1-10 (Table 3 and Fig.6). However, anoxic conditions are also known to favor organic matter preservation and can be recorded by high TOC content (Algeo and Liu, 2020; Schlanger and Jenkyns, 1976), which is not the case for the AR1-10 sample that has one of the lowest TOC content among the analyzed samples (i.e. 0.5%, Table 2). Rather, the samples with the highest TOC content (TOC>2%, Table 1) have lowest Eu/Eu* ratios (0.72-0.88, Table 3) suggesting that diagenetic remobilization of Eu under reducing condition was negligible in our samples.

5.2. Provenance interpretation

Most of the $\delta^{13}C_{TOC}$ values of analyzed samples have organic matter mainly of terrestrial origin because they have $\delta^{13}C_{TOC}$ values within the range of C3 plant-derivated organic matter (-29.3 to −25.5‰, mean~27‰ (e.g. (Tyson, 1995) and depart from typical marine $\delta^{13}C_{TOC}$ values (-18 to−22‰ (e.g.(Meyers, 1997)). Hence, this suggests that the analyzed sedimentary rocks were mainly fed by continental detritus.

The potential sources of the studied sediments may include the rocks of the Guiana Shield, Northwestern Africa, the proto Andes and the Caribbean Large Igneous Province magmatic rocks. Here, we argue that a northwestern African provenance is unlikely because existence of bottom currents parallel to the northwestern African coast during the Cretaceous (Mourlot et al., 2018b) may have prevented the arrival of northwestern African detritus to the deep distal part of the Central Atlantic Ocean (Mourlot et al., 2018b). In addition, aerial transport from northwest Africa is also unlikely because $\varepsilon_{Nd(0)}$ values of our analyzed sedimentary rocks and those of the Demerara rise (Martin et al., 2010) show significant differences with those of contemporaneous sedimentary rocks deposited in the deep offshore Central Atlantic Ocean and northwestern African margin during the Albian-Maastrichtian times (Mourlot et al., 2018a). A proto-Andean provenance is not supported by the provenance of Cretaceous sedimentary rocks deposited in the Amazonian retroarc foreland basin because these sedimentary rocks are cratonic in provenance and were deposited by cratonic paleodrainage (Erlich et al., 2018; George et al., 2019; Hurtado et al., 2018; Louterbach et al., 2018) with very negative $\varepsilon_{Nd(0)}$ values (Hurtado et al., 2018; Louterbach et al., 2018) originated from the Central part of the Amazon Shield (Hurtado et al., 2018).

When plotted on a $^{87}Sr/^{86}Sr$ vs. $\varepsilon_{Nd(0)}$ diagram (Fig. 8) and compared with relevant end-members, including the Precambrian units of the Guiana Shield, the Jurassic mafic dykes related to the CAMP, marine sediments of the Demerara rise and abyssal plain and Suspended Particulate Matters (SPM) transported by modern rivers draining the northern part of South America and the Andes, three groups can be distinguished based on their differences in $\varepsilon_{Nd(0)}$ values.

The first group includes the samples AR1-1 (Early Cretaceous), AR1-9 (Cenomanian) and AR1-23 (Late Campanian) and is characterized by $\varepsilon_{Nd(0)}$ values >-2.2 close to the mean $\varepsilon_{Nd(0)}$ value of the Jurassic mafic dykes (JMD) (i.e. mean= 0.4 Standard Deviation= 3.1, Table S1 (Deckart et al., 2005; Min et al., 2013) and close to Precambrian Avanavero Mafic Intrusions (PMI) (Hebeda et al., 1973; Leal et al., 2012), and some tholeiitic and komatiitic rocks of the Paleoproterozic greenstone belts (GB) (Gruau et al., 1985; Kaminsky et al., 2004; McReath and Faraco, 2005; Voicu et al., 2000) (Figs. 3 and 9). Hence, these high $\varepsilon_{Nd(0)}$ values could indicate provenance from Precambrian or Jurassic mafic source outcropping in the northernmost parts of the Guiana Shield. Alternatively, these high $\varepsilon_{Nd(0)}$ values could also attest to the presence of active basic volcanism during the deposition of analyzed samples.

The two oldest Early Cretaceous (AR1-1) and Cenomanian (AR1-9) samples have trace elements ratios typical of "basic" sediments (i.e., sediments derived from a basic source *sensu* Cullers (2000)), with Eu/Eu* >0.70, Th/Sc<0.4 and Cr/Th > 22.2 (Table 3 and Fig. 6). From a geochemical point of view, it is not possible to distinguish between the Precambrian or Jurassic mafic rocks outcropping in the Guiana Shield and basic volcanism originated from the CLIP, Bahamas hot spot or Apoteri volcanism from the Takutu rift. The AR1-9 sample is marked by a positive $\varepsilon_{Nd(0)}$ excursions of +17.8 to 18.2 units when compared with overlying AR1-8 and underlying AR1-10 samples respectively (Fig. 6 and Table 4). We believe that these positive

$\varepsilon_{Nd(0)}$ excursions sample cannot be explained by a contribution of Precambrian or Jurassic mafic rocks of the Guiana Shield and may favor a basic volcanic source for AR1-9 sample. In effect, Precambrian and Jurassic mafic rocks of the Guiana Shield always outcrop as patches in more differentiated magmatic rocks (Fig. 3) and it is likely that admixture of sediments derived from mafic and more differentiated sources would have resulted in a more negative $\varepsilon_{Nd(0)}$ value for AR1-9 sample. In addition, if mafic rocks outcropping in the Guiana Shield would have been eroded alone, the process leading to the erosion of these rocks would have to be progressive and this would be reflected by a progressive shift toward the highest εNd(0) values and not a positive $\varepsilon_{Nd(0)}$ excursions of +17.8 to 18.2 units. Hence, we favor a Cenomanian basaltic volcanic source for sample AR1-9. Potential candidates may include the basic volcanism of the Caribbean Large Igneous Province (CLIP) active between 94 and 63 Ma (Loewen et al., 2013), or the basic volcanism of the Apoteri volcanic Formation outcropping in the Takutu rift (Crawford et al., 1985). Regarding the latter potential source, Proterozoic or Jurassic ages are generally ascribed to the basaltic flows (Crawford et al., 1985). However, two K/Ar dating measured on basaltic lava flows yield Early Cretaceous ages at 114 ± 3 Ma and 116 ± 4 Ma (Berrangé and Dearnley, 1975,) so that a Cretaceous age for the Apoteri basaltic flow might be possible. However, a volcanic basaltic source might not be true for the oldest Early Cretaceous sample AR1-1. This sample is the only sample analyzed below the Late Albian unconformity (Figs 2 and 6) and because of this low sampling resolution, it is not possible to discard a progressive shift of εNd(0) values. Hence, both contemporaneous basic volcanic rocks and mafic rocks of the Guiana Shield are possible sources for this sample. Potential volcanic source for this sample include the basic volcanism from the CLIP or the Apoteri Formation as well as Aptian-Albian volcanism found on the Guinea Plateau (Olyphant et al., 2017).

The Late Campanian sample (AR1-23) has trace element ratios characteristics of felsic sediments *sensu* (Cullers, 2000) with Eu/Eu* <0.70, Th/Sc>0.64 and Cr/Th < 14.9 (Table 3 and Fig. 6). These exclude mafic sources or basic volcanism as potential sources for this sample and suggest an origin linked to a more acid volcanic activity. The only regional source for this acid volcanism would be the pyroclastic flow recorded in the upper part of the Takutu Formation of the Takutu basin (Crawford et al., 1985). These pyroclastic flows have up to 87% of SiO_2 content but have never been dated. In fact, there is no radiometric nor biostratigraphic dating for the Takutu Formation and for the underlying and overlying formations. Even the positions of the Jurassic/Cretaceous and Cretaceous/Cenozoic boundaries are not constrained. Hence, a Late Cretaceous age for the Takutu Formation cannot be excluded and, in the absence of other option, the pyroclastic flows mentioned at the top of the formation could be the source of the Late Campanian sample.

The second group consists of AR1-11E (Cenomanian) and AR1-21 (Santonian-Campanian) samples and is characterized by intermediate $\varepsilon_{Nd(0)}$ values (-12.2 and – 13.6 respectively, Figs. 6 and 8 and Table 4). In the case of Amazonian sediments, this $\varepsilon_{Nd(0)}$ value is generally used as a cutoff value for identifying more radiogenic Andean-derived sediments (Figueiredo et al., 2009; Horbe et al., 2014; Hurtado et al., 2018; Roddaz et al., 2005). The Sr-Nd isotopic composition of Amazonian Andean sediments is commonly interpreted to reflect mixing between two end-members: the juvenile primitive Andean Arc and the older upper continental crust of the Brazilian shield (Basu et al., 1990; Roddaz et al., 2005). Applying this finding to our results suggests that the two analyzed samples with intermediate $\varepsilon_{Nd(0)}$ values might result from mixing between the northern mafic sources listed above (i.e., JMD, PMI and GB) or basic volcanic sources (CLIP, Bahamas hot spot or Apoteri volcanism) and the differentiated

Precambrian granitoids and metamorphic rocks (e.g., PGGF, PHGB) (Fig. 8). However, more samples are needed to test a mixing hyperbole between these two end-members.

The third group of samples encompasses all other analyzed and is characterized by $\varepsilon_{Nd(0)}$ values inferior to -15.8 with a median $\varepsilon_{Nd(0)}$ value at -19.2 (Table 4, Fig. 8). Such low $\varepsilon_{Nd(0)}$ values are typical of Amazonian cratonic-derived sedimentary rocks and present-day cratonic-derived river sediments (e.g., Maroni, upper Orinoco, Trombetas rivers) dominated by supplies from Paleoproterozoic and Mesoproterozoic granites, gneiss and metamorphic series (PFFG) covering the more inner parts of the craton (Figs. 3 and 8) (Allègre et al., 1996; Goldstein et al. 1997; Bayon et al., 2015; Figueiredo et al., 2009; Roddaz et al., 2005). For instance, Suspended Particulate Matter (SPM) transported by the Maroni River draining the Paleoproterozoic terranes to the east of the Guiana shield have $\varepsilon_{Nd(0)}$ values between -21 and -25.2 (Rousseau et al., 2019) (Fig. 3 and 8). Compared with the modern Maroni SPM, the Cretaceous sediments from the Guyana-Suriname basin have a slightly more juvenile Nd isotopic ratios but they have similar $\varepsilon_{Nd(0)}$ values as the Upper Orinoco river fine-grained sediments analyzed in Goldstein et al. 1997 (-19.6 and -20.5 respectively, Table S1) suggesting a similar origin (Fig. 3).

Based on their $\varepsilon_{Nd(0)}$ values, most of the analyzed samples derive from the Guiana Shield with variable contributions from two main sources: 1) Paleoproterozoic granitic and metamorphic units covering the innermost parts of the shield and 2) Jurassic or Precambrian mafic dykes and greenstone belts. More insight can be gained with trace elements ratios and $^{87}Sr/^{86}Sr$ isotopic ratios. For instance, the four Late Santonian to Paleocene samples have more radiogenic $^{87}Sr/^{86}Sr$ ratios than the oldest samples. These younger samples have Eu/Eu*, Th/Sc and Cr/Th ratios close to that of the PAAS whereas oldest samples have Eu/Eu*, Th/Sc and Cr/Th ratios close to those defining “basic sediments” sensu Cullers (2000) (Fig. 6). As there is

no coeval change in $\varepsilon_{Nd(0)}$ values, these temporal changes in trace elements ratios and $^{87}Sr/^{86}Sr$ isotopic ratios could result from increasing contributions of more felsic sources rather than contribution from older sources. Potential candidates for these felsic sources could be Paleoproterozoic granitoids, gneiss and felsic volcanic units, Mezoproterozoic granites, or high-grade granulite belts (PGGF, MG, PHGB in Fig. 3 respectively). Both units outcrop in the inner part of the Guiana Shield and thus imply an extension of the drainage area toward the South between the Coniacian and the Santonian (Fig. 9).

5.3 Implications for the Late Cretaceous evolution of Atlantic equatorial margins

Our geochemical data support that Early Cretaceous-Paleocene sediments of the Guyana-Suriname basin have a Guiana cratonic provenance. Analysis of 2D seismic lines suggest that the deep offshore part of the Guyana-Suriname basin was supplied by these cratonic sediments via a large canyon system fed by the proto-Berbice river (Figs.1 and 9) with a paleo-delta probably located between the present-day Berbice and Corantijn rivers (Erlich and Keens-Dumas 2007; Mourlot, 2018; Yang and Escalona, 2011). Our provenance data also suggests an extension of the proto-Berbice drainage area toward the inner parts of the Guiana craton after the Coniacian (~86 Ma, Fig. 9), likely through the Takutu rift. This provenance change was associated with a decrease in TOC content and a six fold increase in sedimentation rate in the Arapaima-1 well (Mourlot, 2018), suggesting increasing erosion of inner parts of the Guiana Shield. Geomorphological and thermochronological data also attest to uplift and erosion of the inner domains of the Guiana Shield during the Late Cretaceous (Sapin et al., 2016). In the easternmost part of Suriname and in Brazil (close to the Brazilian-Suriname frontier) (see Fig. 7 in Sapin et al., 2016), a Late Cretaceous erosive surface ("peneplanation surface") termed S0 exposed at elevation > ~ 900 m above sea level (asl) has been identified and mapped (Sapin et al., 2016).

This surface was dated by Ar/Ar on lateritic material at ~71 Ma and Apatite Fission Track Analysis at 77 ± 3 Ma (Sapin et al., 2016 and references therein) suggesting that a significant erosion affected this part of the craton during the Campanian. This S0 surface outcrops immediately above the PGGF basement and hence has recorded the uplift and erosion of this terrane, which would be consistent with the increasing contribution of a felsic source to the Late Santonian-Paleocene sediments. This post Coniacian uplift of the Guiana Shield post-dated by >20 Ma the post-rift Albian tectonic inversion ascribed to a plate kinematic change that affected the Demerara Plateau (offshore French Guiana) at *ca* 105 Ma (Basile et al., 2013). In northeastern Brazil, various studies have presented evidences for a Late Cretaceous uplift (Harman et al., 1998; Morais Neto et al., 2009; Peulvast and Bétard, 2015; Potter, 1997). Increase of denudation at ~80–60 Ma of the eastern Central Brazilian shield is documented by thermal histories derived from fission track data (Harman et al., 1998). This uplift and erosion of the Central Brazilian shield is also attested by the development of the high elevated (~720 m asl) Brazilian Carajas surface in northeastern Amazonia which started its weathering history at *ca.* 80 Ma (Monteiro et al., 2018). Late Cretaceous fission track cooling ages (Morais Neto et al., 2009) as well as presence of Cenomanian marine deposits associated to development of Paleogene laterites on the top of the Borborema Plateau (Peulvast and Bétard, 2015) indicate that the Borborema plateau (Northeastern Brazil) underwent uplift and denudation between the Cenomanian and Early Cenozoic. In the conjugate margin of NW Africa, the Campanian−Maastrichtian is characterized by increasing input of Precambrian detritus along the Northwest African Margin and a progression of drainage areas toward the east and the inner units of the West African Craton (Mourlot et al., 2018a).

Based on this literature review, both the northeastern South American and West African cratons experienced coeval post Coniacian uplift of their inner parts suggesting that a similar post-rift geodynamic mechanism occurred during the opening of the Atlantic Equatorial Ocean. This coeval uplift of the Atlantic margins could result from significant intracontinental deformation caused by major change in the relative plate motions between Africa, Antarctica, and South America that began between anomaly C34 (83 Ma) and C31 (67 Ma) (see Harman et al., 1998 and references therein) as well as mantle upwelling under the margin (Matton and Jébrak, 2009) or a combination of these. Furthermore, given the presence of a volcanic eruption in the Late Campanian as recorded by the sample AR1-23, the presence of an active plume mantle upwelling cannot be discarded.

6. Conclusions

Based on the TOC content, $\delta^{13}C_{TOC}$ data, major and trace element concentrations and Sr–Nd isotopic compositions of Cretaceous to Paleocene sedimentary rocks sampled in the Arapaima-1 well (Guyana-Suriname basin) compared with an extensive Sr-Nd isotopic composition of possible sources, this provenance study yields the following conclusions:

- Three samples AR1-1 ((Early Cretaceous, AR1-9 (Cenomanian,) and AR1-23 (Late Campanian in age) have $\varepsilon_{Nd(0)}$ values >-2.2 that might have recorded volcanic activity during their deposition. However, this interpretation might not be true for the oldest sample AR1-1 that could also be sourced by mafic rocks from the Guiana Shield. The Cenomanian sample may have recorded basic volcanic activity of the Caribbean Large Igneous Province or the Takutu rift, whereas the Late Campanian sample would record acid volcanic eruption associated with the pyroclastic flow having affected the Takutu rift in the Cretaceous;

- All other analyzed samples have an overall Guiana cratonic provenance with variable contributions from Paleoproterozoic and Mesoproterozoic and greenstone belt, Jurassic and Precambrian mafic dykes. Two Cenomanian and Santonian-Campanian samples (AR1-11F and AR1-21) have intermediate $\varepsilon_{Nd(0}$ values of ~ -13 suggesting more important contribution of mafic rocks from the Guiana Shield or basic volcanic rocks from the CLIP, Bahamas hot spot or Apoteri volcanism. The other samples have $\varepsilon_{Nd(0}$ <-15.8 and suggest a dominant provenance from the inner Paleoproterozoic granitic units of the Guiana Shield;
- Late Santonian to Paleocene samples have more radiogenic $^{87}Sr/^{86}Sr$ isotopic ratios and trace element ratios characteristic of more differentiated sources when compared with oldest samples. This suggests an increasing contribution from the Paleoproterozoic granitoids, gneiss and felsic volcanism units or the Mesoproterozoic granites through time. This also implies an evolution of the drainage area toward the inner parts of the Guiana Shield between the Coniacian and the Santonian.

This post-Coniacian erosion of the inner parts of the Guiana Shield is recorded in various other parts of the northeastern South American and West African cratons. This suggests that they experienced a similar uplift mechanism occurring during the opening of the Atlantic Equatorial Ocean. Probable causes could be a major change in the relative plate motions between Africa and South America as well as post rift mantle upwelling under the margin. The latter hypothesis could be favored by the supposed presence of active volcanism during the deposition of the analyzed samples.

Acknowledgments

This study was funded by Total Exploration and Production through the R&D project "Sedimentology of organic matter in deep oceanic basins" (TOTAL: FR00007862 and CNRS 122560). Jung-Hyun Kim was also partly supported by a grant from the National Research Foundation of Korea (NRF) funded by the Korea government (MSIP) (No.2016R1A2B3015388) and a project from the Korean Government (MSIT) (NRF-2015M1A5A1037243, KOPRI-PN20090). This work was part of Yannick Mourlot PhD thesis funded by Total E&P. We thank three anonymous reviewers as well as the editor Adina Paytan for valuable reviews that improved this contribution.

Data availability

All geochemical data including total organic carbon (TOC) content, $\delta^{13}C_{TOC}$, major and trace element concentrations, and Sr-Nd isotopic data (Table 2 to 4) as well as compiled database, major and trace element uncertainties and correlation coefficients (Table S1 to S3) are uploaded into an online supplementary dataset associated with this paper (Roddaz, Martin; Dera, Guillaume; Mourlot, Yannick; Calves, Gerome; Kim, Jung-Hyun; Chaboureau, Anne-Claire; Mounic, Stephanie; Raisson, Francois (2020), "Geochemistry of Arapaima well sediments Roddaz et al. in Revision to Marine Geology", Mendeley Data, V2, doi: 10.17632/jnwgsn98tt.2, http://dx.doi.org/10.17632/jnwgsn98tt.2)).

References

Algeo, T.J., Liu, J., 2020. A re-assessment of elemental proxies for paleoredox analysis. Chem. Geol. 540, 119549. https://doi.org/10.1016/j.chemgeo.2020.119549

Allègre, C.J., Dupré, B., Négrel, P., Gaillardet, J., 1996. Sr□Nd□Pb isotope systematics in Amazon and Congo River systems: constraints about erosion processes. Chem. Geol. 131, 93–112. https://doi.org/10.1016/0009-2541(96)00028-9

Andersen, T., Elburg, M.A., Magwaza, B.N., 2019. Sources of bias in detrital zircon geochronology: Discordance, concealed lead loss and common lead correction. Earth-Sci. Rev. 197, 102899. https://doi.org/10.1016/j.earscirev.2019.102899

Barreto, C.J.S., Lafon, J.M., da Rosa Costa, L.T., Dantas, E.L., 2013. Paleoproterozoic granitoids from the northern limit of the Archean Amapá block (Brazil), southeastern Guyana Shield: Pb–Pb evaporation in zircons and Sm–Nd geochronology. J. South Am. Earth Sci. 45, 97–116. https://doi.org/10.1016/j.jsames.2013.02.005

Basile, C., 2015. Transform continental margins — part 1: Concepts and models. Tectonophysics 661, 1–10. https://doi.org/10.1016/j.tecto.2015.08.034

Basile, C., Girault, I., Paquette, J.-L., Agranier, A., Loncke, L., Heuret, A., Poetisi, E., 2020. The Jurassic magmatism of the Demerara Plateau (offshore French Guiana) as a remnant of the Sierra Leone hotspot during the Atlantic rifting. Sci. Rep. 10, 7486. https://doi.org/10.1038/s41598-020-64333-5

Basile, C., Maillard, A., Patriat, M., Gaullier, V., Loncke, L., Roest, W., Mercier de Lépinay, M., Pattier, F., 2013. Structure and evolution of the Demerara Plateau, offshore French Guiana: Rifting, tectonic inversion and post-rift tilting at transform–divergent margins intersection. Tectonophysics, Basin Dynamics 591, 16–29. https://doi.org/10.1016/j.tecto.2012.01.010

Basile, C., Mascle, J., Guiraud, R., 2005. Phanerozoic geological evolution of the Equatorial Atlantic domain. J. Afr. Earth Sci., Phanerozoic Evolution of Africa 43, 275–282. https://doi.org/10.1016/j.jafrearsci.2005.07.011

Basu, A.R., Sharma, M., DeCelles, P.G., 1990. Nd, Sr-isotopic provenance and trace element geochemistry of Amazonian foreland basin fluvial sands, Bolivia and Peru: implications for ensialic Andean orogeny. Earth Planet. Sci. Lett. 100, 1–17. https://doi.org/10.1016/0012-821X(90)90172-T

Bayon, G., German, C.R., Boella, R.M., Milton, J.A., Taylor, R.N., Nesbitt, R.W., 2002. An improved method for extracting marine sediment fractions and its application to Sr and Nd isotopic analysis. Chem. Geol. 187, 179–199. https://doi.org/10.1016/S0009-2541(01)00416-8

Bayon, G., Toucanne, S., Skonieczny, C., André, L., Bermell, S., Cheron, S., Dennielou, B., Etoubleau, J., Freslon, N., Gauchery, T., Germain, Y., Jorry, S.J., Ménot, G., Monin, L., Ponzevera, E., Rouget, M.-L., Tachikawa, K., Barrat, J.A., 2015. Rare earth elements and neodymium isotopes in world river sediments revisited. Geochim. Cosmochim. Acta 170, 17–38. https://doi.org/10.1016/j.gca.2015.08.001

Benkhelil, J., Mascle, J., Tricart, P., 1995. The Guinea continental margin: an example of a structurally complex transform margin. Tectonophysics 248, 117–137. https://doi.org/10.1016/0040-1951(94)00246-6

Berrangé, J.P., Dearnley, R., 1975. The Apoteri volcanic formation — tholeiitic flows in the North Savannas Graben of Guyana and Brazil. Geol. Rundsch. 64, 883–899. https://doi.org/10.1007/BF01820702

Berrocoso, Á.J., MacLeod, K.G., Calvert, S.E., Elorza, J., 2008. Bottom water anoxia, inoceramid colonization, and benthopelagic coupling during black shale deposition on Demerara Rise (Late Cretaceous western tropical North Atlantic). Paleoceanography 23. https://doi.org/10.1029/2007PA001545

Bodin, S., Meissner, P., Janssen, N.M.M., Steuber, T., Mutterlose, J., 2015. Large igneous provinces and organic carbon burial: Controls on global temperature and continental weathering during the Early Cretaceous. Glob. Planet. Change 133, 238–253. https://doi.org/10.1016/j.gloplacha.2015.09.001

Boher, M., Abouchami, W., Michard, A., Albarede, F., Arndt, N.T., 1992. Crustal growth in West Africa at 2.1 Ga. J. Geophys. Res. Solid Earth 97, 345–369. https://doi.org/10.1029/91JB01640

Bouchez, J., Gaillardet, J., France- Lanord, C., Maurice, L., Dutra- Maia, P., 2011. Grain size control of river suspended sediment geochemistry: Clues from Amazon River depth profiles. Geochem. Geophys. Geosystems 12. https://doi.org/10.1029/2010GC003380

Caracciolo, L., 2020. Sediment generation and sediment routing systems from a quantitative provenance analysis perspective: Review, application and future development. Earth-Sci. Rev. 209, 103226. https://doi.org/10.1016/j.earscirev.2020.103226

Chew, D., O'Sullivan, G., Caracciolo, L., Mark, C., Tyrrell, S., 2020. Sourcing the sand: Accessory mineral fertility, analytical and other biases in detrital U-Pb provenance analysis. Earth-Sci. Rev. 202, 103093. https://doi.org/10.1016/j.earscirev.2020.103093

Clift, P.D., Blusztajn, J., 2005. Reorganization of the western Himalayan river system after five million years ago. Nature 438, 1001–1003. https://doi.org/10.1038/nature04379

Cogné, N., Gallagher, K., Cobbold, P.R., Riccomini, C., Gautheron, C., 2012. Post-breakup tectonics in southeast Brazil from thermochronological data and combined inverse-forward thermal history modeling. J. Geophys. Res. Solid Earth 117. https://doi.org/10.1029/2012JB009340

Condie, K.C., 1993. Chemical composition and evolution of the upper continental crust: Contrasting results from surface samples and shales. Chem. Geol. 104, 1–37. https://doi.org/10.1016/0009-2541(93)90140-E

Crawford, F.D., Szelewski, C.E., Alvey, G.D., 1985. Geology and Exploration in the Takutu Graben of Guyana Brazil. J. Pet. Geol. 8, 5–36. https://doi.org/10.1111/j.1747-5457.1985.tb00189.x

Cullers, R.L., 2000. The geochemistry of shales, siltstones and sandstones of Pennsylvanian–Permian age, Colorado, USA: implications for provenance and metamorphic studies. Lithos 51, 181–203. https://doi.org/10.1016/S0024-4937(99)00063-8

da Rosa-Costa, L.T., Lafon, J.M., Delor, C., 2006. Zircon geochronology and Sm–Nd isotopic study: Further constraints for the Archean and Paleoproterozoic geodynamical evolution of the southeastern Guiana Shield, north of Amazonian Craton, Brazil. Gondwana Res. 10, 277–300. https://doi.org/10.1016/j.gr.2006.02.012

De Baar, H.J.W., Bacon, M.P., Brewer, P.G., Bruland, K.W., 1985. Rare earth elements in the Pacific and Atlantic Oceans. Geochim. Cosmochim. Acta 49, 1943–1959. https://doi.org/10.1016/0016-7037(85)90089-4

Deckart, K., Bertrand, H., Liégeois, J.-P., 2005. Geochemistry and Sr, Nd, Pb isotopic composition of the Central Atlantic Magmatic Province (CAMP) in Guyana and Guinea.

Lithos, Isotopes in Igneous Petrogenesis 82, 289–314. https://doi.org/10.1016/j.lithos.2004.09.023

Dera, G., Prunier, J., Smith, P.L., Haggart, J.W., Popov, E., Guzhov, A., Rogov, M., Delsate, D., Thies, D., Cuny, G., Pucéat, E., Charbonnier, G., Bayon, G., 2015. Nd isotope constraints on ocean circulation, paleoclimate, and continental drainage during the Jurassic breakup of Pangea. Gondwana Res. 27, 1599–1615. https://doi.org/10.1016/j.gr.2014.02.006

Dickinson, W.R., 2008. Impact of differential zircon fertility of granitoid basement rocks in North America on age populations of detrital zircons and implications for granite petrogenesis. Earth Planet. Sci. Lett. 275, 80–92. https://doi.org/10.1016/j.epsl.2008.08.003

Dickinson, W.R., 1985. Interpreting Provenance Relations from Detrital Modes of Sandstones, in: Zuffa, G.G. (Ed.), Provenance of Arenites, NATO ASI Series. Springer Netherlands, Dordrecht, pp. 333–361. https://doi.org/10.1007/978-94-017-2809-6_15

Dickinson, W.R., Suczek, C.A., 1979. Plate Tectonics and Sandstone Compositions. AAPG Bull. 63, 2164–2182. https://doi.org/10.1306/2F9188FB-16CE-11D7-8645000102C1865D

Donnadieu, Y., Pucéat, E., Moiroud, M., Guillocheau, F., Deconinck, J.-F., 2016. A better-ventilated ocean triggered by Late Cretaceous changes in continental configuration. Nat. Commun. 7, 1–12. https://doi.org/10.1038/ncomms10316

Emery, K.O., Uchupi, E., Phillips, J., Bowin, C., Mascle, J., 1975. Continental Margin Off Western Africa: Angola to Sierra Leone. AAPG Bull. 59, 2209–2265. https://doi.org/10.1306/83D92249-16C7-11D7-8645000102C1865D

Erlich, R.N., Fallon, J., O'Sullivan, P., 2018. Stratigraphy and LA-ICP-MS zircon U-PB provenance of middle Permian to Maastrichtian sandstones from outcrop and subsurface

control in the sub-Andean basins of Peru, in: Petroleum Basins and Hydrocarbon Potential of the Andes of Peru and Bolivia, AAPG Memoirs. AAPG, pp. 175–222.

Fedo, C.M., Nesbitt, H.W., Young, G.M., 1995. Unraveling the effects of potassium metasomatism in sedimentary rocks and paleosols, with implications for paleoweathering conditions and provenance. Geology 23, 921–924. https://doi.org/10.1130/0091-7613(1995)023<0921:UTEOPM>2.3.CO;2

Figueiredo, J., Hoorn, C., Ven, P. van der, Soares, E., 2009. Late Miocene onset of the Amazon River and the Amazon deep-sea fan: Evidence from the Foz do Amazonas Basin. Geology 37, 619–622. https://doi.org/10.1130/G25567A.1

Friedrich, O., Norris, R.D., Erbacher, J., 2012. Evolution of middle to Late Cretaceous oceans—A 55 m.y. record of Earth's temperature and carbon cycle. Geology 40, 107–110. https://doi.org/10.1130/G32701.1

Gallagher, K., Brown, R., 1999. The Mesozoic denudation history of the Atlantic margins of southern Africa and southeast Brazil and the relationship to offshore sedimentation. Geol. Soc. Lond. Spec. Publ. 153, 41–53. https://doi.org/10.1144/GSL.SP.1999.153.01.03

Gallagher, K., Hawkesworth, C.J., Mantovani, M.S.M., 1994. The denudation history of the onshore continental margin of SE Brazil inferred from apatite fission track data. J. Geophys. Res. Solid Earth 99, 18117–18145. https://doi.org/10.1029/94JB00661

Garzanti, E., 2019. Petrographic classification of sand and sandstone. Earth-Sci. Rev. 192, 545–563. https://doi.org/10.1016/j.earscirev.2018.12.014

Garzanti, E., 2016. From static to dynamic provenance analysis—Sedimentary petrology upgraded. Sediment. Geol., Sediment generation and provenance: processes and pathways 336, 3–13. https://doi.org/10.1016/j.sedgeo.2015.07.010

Garzanti, E., Andò, S., 2019. Heavy Minerals for Junior Woodchucks. Minerals 9, 148. https://doi.org/10.3390/min9030148

Garzanti, E., Andò, S., Vezzoli, G., 2009. Grain-size dependence of sediment composition and environmental bias in provenance studies. Earth Planet. Sci. Lett. 277, 422–432. https://doi.org/10.1016/j.epsl.2008.11.007

Garzanti, E., Andò, S., Vezzoli, G., 2008. Settling equivalence of detrital minerals and grain-size dependence of sediment composition. Earth Planet. Sci. Lett. 273, 138–151. https://doi.org/10.1016/j.epsl.2008.06.020

Garzanti, E., Padoan, M., Setti, M., López-Galindo, A., Villa, I.M., 2014. Provenance versus weathering control on the composition of tropical river mud (southern Africa). Chem. Geol. 366, 61–74. https://doi.org/10.1016/j.chemgeo.2013.12.016

Gaudette, H.E., Mendoza, V., Hurley, P.M., Fairbairn, H.W., 1978. Geology and age of the Parguaza rapakivi granite, Venezuela. GSA Bull. 89, 1335–1340. https://doi.org/10.1130/0016-7606(1978)89<1335:GAAOTP>2.0.CO;2

Gaudette, H.E., Olszewski, W.J., Santos, J.O.S., 1996. Geochronology of Precambrian rocks from the northern part of the Guiana Shield, State of Roraima, Brazil. J. South Am. Earth Sci. 9, 183–195. https://doi.org/10.1016/0895-9811(96)00005-3

George, S.W.M., Horton, B.K., Jackson, L.J., Moreno, F., Carlotto, V., Garzione, C.N., 2019. Chapter 10 - Sediment provenance variations during contrasting Mesozoic-early Cenozoic tectonic regimes of the northern Peruvian Andes and Santiago-Marañón foreland basin, in: Horton, B.K., Folguera, A. (Eds.), Andean Tectonics. Elsevier, pp. 269–296. https://doi.org/10.1016/B978-0-12-816009-1.00012-5

Gibbs, A.K., Montgomery, C.W., O'Day, P.A., Erslev, E.A., 1986. The Archean-Proterozoic transition: Evidence from the geochemistry of metasedimentary rocks of Guyana and Montana. Geochim. Cosmochim. Acta 50, 2125–2141. https://doi.org/10.1016/0016-7037(86)90067-0

Goldstein, S.L., Arndt, N.T., Stallard, R.F., 1997. The history of a continent from U□Pb ages of zircons from Orinoco River sand and Sm□Nd isotopes in Orinoco basin river sediments. Chem. Geol. 139, 271–286. https://doi.org/10.1016/S0009-2541(97)00039-9

Gouyet, S., Unternehr, P., Mascle, A., 1994. The French Guyana Margin and the Demerara Plateau: Geological History and Petroleum Plays, in: Mascle, Alain (Ed.), Hydrocarbon and Petroleum Geology of France, Special Publication of the European Association of Petroleum Geoscientists. Springer, Berlin, Heidelberg, pp. 411–422. https://doi.org/10.1007/978-3-642-78849-9_29

Gruau, G., Martin, H., Leveque, B., Capdevila, R., Marot, A., 1985. Rb—Sr and Sm—Nd geochronology of lower Proterozoic granite—greenstone terrains in French Guiana, South America. Precambrian Res. 30, 63–80. https://doi.org/10.1016/0301-9268(85)90029-4

Hall, S.A., Bird, D.E., McLean, D.J., Towle, P.J., Grant, J.V., Danque, H.A., 2018. New constraints on the age of the opening of the South Atlantic basin. Mar. Pet. Geol. 95, 50–66. https://doi.org/10.1016/j.marpetgeo.2018.03.010

Harman, R., Gallagher, K., Brown, R., Raza, A., Bizzi, L., 1998. Accelerated denudation and tectonic/geomorphic reactivation of the cratons of northeastern Brazil during the Late Cretaceous. J. Geophys. Res. Solid Earth 103, 27091–27105. https://doi.org/10.1029/98JB02524

Hebeda, E.H., Boelrijk, N.A.I.M., Priem, H.N.A., Verdurmen, E.A.Th., Verschure, R.H., 1973. Excess radiogenic argon in the Precambrian Avanavero Dolerite in western Suriname (South America). Earth Planet. Sci. Lett. 20, 189–200. https://doi.org/10.1016/0012-821X(73)90157-X

Heine, C., Zoethout, J., Müller, R.D., 2013. Kinematics of the South Atlantic rift. Solid Earth 4, 215–253. https://doi.org/10.5194/se-4-215-2013

Heinonen, A.P., Fraga, L.M., Rämö, O.T., Dall'Agnol, R., Mänttäri, I., Andersen, T., 2012. Petrogenesis of the igneous Mucajaí AMG complex, northern Amazonian craton — Geochemical, U–Pb geochronological, and Nd–Hf–O isotopic constraints. Lithos, A-type granites and related rocks through time 151, 17–34. https://doi.org/10.1016/j.lithos.2011.07.016

Hetzel, A., Böttcher, M.E., Wortmann, U.G., Brumsack, H.-J., 2009. Paleo-redox conditions during OAE 2 reflected in Demerara Rise sediment geochemistry (ODP Leg 207). Palaeogeogr. Palaeoclimatol. Palaeoecol., Organic-carbon-rich sediments through the Phanerozoic: Processes, progress, and perspectives 273, 302–328. https://doi.org/10.1016/j.palaeo.2008.11.005

Hiruma, S.T., Riccomini, C., Modenesi-Gauttieri, M.C., Hackspacher, P.C., Neto, J.C.H., Franco-Magalhães, A.O.B., 2010. Denudation history of the Bocaina Plateau, Serra do Mar, southeastern Brazil: Relationships to Gondwana breakup and passive margin development. Gondwana Res. 18, 674–687. https://doi.org/10.1016/j.gr.2010.03.001

Hodell, D.A., Kamenov, G.D., Hathorne, E.C., Zachos, J.C., Röhl, U., Westerhold, T., 2007. Variations in the strontium isotope composition of seawater during the Paleocene and

early Eocene from ODP Leg 208 (Walvis Ridge). Geochem. Geophys. Geosystems 8. https://doi.org/10.1029/2007GC001607

Horbe, A.M.C., da Trindade, I.R., Dantas, E.L., Santos, R.V., Roddaz, M., 2014. Provenance of quaternary and modern alluvial deposits of the Amazonian floodplain (Brazil) inferred from major and trace elements and Pb–Nd–Sr isotopes. Palaeogeogr. Palaeoclimatol. Palaeoecol. 411, 144–154. https://doi.org/10.1016/j.palaeo.2014.06.019

Huck, C.E., Flierdt, T. van de, Jiménez- Espejo, F.J., Bohaty, S.M., Röhl, U., Hammond, S.J., 2016. Robustness of fossil fish teeth for seawater neodymium isotope reconstructions under variable redox conditions in an ancient shallow marine setting. Geochem. Geophys. Geosystems 17, 679–698. https://doi.org/10.1002/2015GC006218

Hurley, P.M., Melcher, G.C., Pinson Jr., W.H., Fairbairn, H.W., 1968. Some orogenic episodes in South America by K–Ar and whole-rock Rb–Sr dating. Can. J. Earth Sci. 5, 633–638. https://doi.org/10.1139/e68-059

Hurtado, C., Roddaz, M., Santos, R.V., Baby, P., Antoine, P.-O., Dantas, E.L., 2018. Cretaceous-early Paleocene drainage shift of Amazonian rivers driven by Equatorial Atlantic Ocean opening and Andean uplift as deduced from the provenance of northern Peruvian sedimentary rocks (Huallaga basin). Gondwana Res. 63, 152–168. https://doi.org/10.1016/j.gr.2018.05.012

Jacobsen, S.B., Wasserburg, G.J., 1980. Sm-Nd isotopic evolution of chondrites. Earth Planet. Sci. Lett. 50, 139–155. https://doi.org/10.1016/0012-821X(80)90125-9

Japsen, P., Bonow, J.M., Green, P.F., Cobbold, P.R., Chiossi, D., Lilletveit, R., Magnavita, L.P., Pedreira, A., 2012. Episodic burial and exhumation in NE Brazil after opening of the South Atlantic. GSA Bull. 124, 800–816. https://doi.org/10.1130/B30515.1

Jeandel, C., Arsouze, T., Lacan, F., Téchiné, P., Dutay, J.-C., 2007. Isotopic Nd compositions and concentrations of the lithogenic inputs into the ocean: A compilation, with an emphasis on the margins. Chem. Geol. 239, 156–164. https://doi.org/10.1016/j.chemgeo.2006.11.013

Jeandel, C., Oelkers, E.H., 2015. The influence of terrigenous particulate material dissolution on ocean chemistry and global element cycles. Chem. Geol. 395, 50–66. https://doi.org/10.1016/j.chemgeo.2014.12.001

Jelinek, A.R., Chemale, F., van der Beek, P.A., Guadagnin, F., Cupertino, J.A., Viana, A., 2014. Denudation history and landscape evolution of the northern East-Brazilian continental margin from apatite fission-track thermochronology. J. South Am. Earth Sci. 54, 158–181. https://doi.org/10.1016/j.jsames.2014.06.001

Kaminsky, F.V., Sablukov, S.M., Sablukova, L.I., Channer, D.M.DeR., 2004. Neoproterozoic ‘anomalous’ kimberlites of Guaniamo, Venezuela: Mica kimberlites of ‘isotopic transitional’ type. Lithos, Selected Papers from the Eighth International Kimberlite Conference. Volume 1: The C. Roger Clement Volume 76, 565–590. https://doi.org/10.1016/j.lithos.2004.03.035

Klaver, M., de Roever, E.W.F., Nanne, J.A.M., Mason, P.R.D., Davies, G.R., 2015. Charnockites and UHT metamorphism in the Bakhuis Granulite Belt, western Suriname: Evidence for two separate UHT events. Precambrian Res. 262, 1–19. https://doi.org/10.1016/j.precamres.2015.02.014

Kroonenberg, S.B., Roever, E.W.F. de, Fraga, L.M., Reis, N.J., Faraco, T., Lafon, J.-M., Cordani, U., Wong, T.E., 2016. Paleoproterozoic evolution of the Guiana Shield in

Suriname: A revised model. Neth. J. Geosci. 95, 491–522. https://doi.org/10.1017/njg.2016.10

Larson, R.L., 1991. Latest pulse of Earth: Evidence for a mid-Cretaceous superplume. Geology 19, 547–550. https://doi.org/10.1130/0091-7613(1991)019<0547:LPOEEF>2.3.CO;2

Lawrence, R.L., Cox, R., Mapes, R.W., Coleman, D.S., 2011. Hydrodynamic fractionation of zircon age populations. GSA Bull. 123, 295–305. https://doi.org/10.1130/B30151.1

Leal, A.B.M., Girardi, V. a. V., Leal, L.R.B., 2012. GEOLOGIA, PETROGRAFIA E GEOQUÍMICA DOS SILLS COTINGO E PEDRA PRETA, ESTADO DE RORAIMA, BRASIL. Geochim. Bras. 20, 233–250. https://doi.org/10.21715/gb.v20i3.247

Lenharo, S.L.R., Moura, M.A., Botelho, N.F., 2002. Petrogenetic and mineralization processes in Paleo- to Mesoproterozoic rapakivi granites: examples from Pitinga and Goiás, Brazil. Precambrian Res. 119, 277–299. https://doi.org/10.1016/S0301-9268(02)00126-2

Loewen, M.W., Duncan, R.A., Kent, A.J.R., Krawl, K., 2013. Prolonged plume volcanism in the Caribbean Large Igneous Province: New insights from Curaçao and Haiti. Geochem. Geophys. Geosystems 14, 4241–4259. https://doi.org/10.1002/ggge.20273

Loncke, L., Roest, W.R., Klingelhoefer, F., Basile, C., Graindorge, D., Heuret, A., Marcaillou, B., Museur, T., Fanget, A.S., Mercier de Lépinay, M., 2019. Transform marsginal plateaus. Earth-Sci. Rev. 102940. https://doi.org/10.1016/j.earscirev.2019.102940

Louterbach, M., Roddaz, M., Antoine, P.-O., Marivaux, L., Adnet, S., Bailleul, J., Dantas, E., Santos, R.V., Chemale, F., Baby, P., Sanchez, C., Calderon, Y., 2018. Provenance record of late Maastrichtian–late Palaeocene Andean Mountain building in the Amazonian retroarc foreland basin (Madre de Dios basin, Peru). Terra Nova 30, 17–23. https://doi.org/10.1111/ter.12303

MacRae, N.D., Nesbitt, H.W., Kronberg, B.I., 1992. Development of a positive Eu anomaly during diagenesis. Earth Planet. Sci. Lett. 109, 585–591. https://doi.org/10.1016/0012-821X(92)90116-D

Malusà, M.G., Carter, A., Limoncelli, M., Villa, I.M., Garzanti, E., 2013. Bias in detrital zircon geochronology and thermochronometry. Chem. Geol. 359, 90–107. https://doi.org/10.1016/j.chemgeo.2013.09.016

Malusà, M.G., Resentini, A., Garzanti, E., 2016. Hydraulic sorting and mineral fertility bias in detrital geochronology. Gondwana Res. 31, 1–19. https://doi.org/10.1016/j.gr.2015.09.002

Mann, P., Taylor, F.W., Edwards, R.L., Ku, T.-L., 1995. Actively evolving microplate formation by oblique collision and sideways motion along strike-slip faults: An example from the northeastern Caribbean plate margin. Tectonophysics 246, 1–69. https://doi.org/10.1016/0040-1951(94)00268-E

Marques, S.N. de S., Souza, V. da S., Dantas, E.L., Valério, C. da S., Nascimento, R.S.C. do, 2014. Contribuições para a petrografia, geoquímica e geocronologia (U-Pb e Sm-Nd) das rochas efusivas Paleoproterozóicas do Grupo Iricoumé, craton Amazônico, Brasil. Braz. J. Geol. 44, 121–138. https://doi.org/10.5327/Z2317-4889201400010010

Martin, E.E., Blair, S.W., Kamenov, G.D., Scher, H.D., Bourbon, E., Basak, C., Newkirk, D.N., 2010. Extraction of Nd isotopes from bulk deep sea sediments for paleoceanographic studies on Cenozoic time scales. Chem. Geol. 269, 414–431. https://doi.org/10.1016/j.chemgeo.2009.10.016

Martin, E.E., MacLeod, K.G., Jiménez Berrocoso, A., Bourbon, E., 2012. Water mass circulation on Demerara Rise during the Late Cretaceous based on Nd isotopes. Earth Planet. Sci. Lett. 327–328, 111–120. https://doi.org/10.1016/j.epsl.2012.01.037

Marzoli, A., Renne, P.R., Piccirillo, E.M., Ernesto, M., Bellieni, G., Min, A.D., 1999. Extensive 200-Million-Year-Old Continental Flood Basalts of the Central Atlantic Magmatic Province. Science 284, 616–618. https://doi.org/10.1126/science.284.5414.616

Mascle, J., Blarez, E., 1987. Evidence for transform margin evolution from the Ivory Coast–Ghana continental margin. Nature 326, 378–381. https://doi.org/10.1038/326378a0

McLennan, S.M., 1989. Rare earth elements in sedimentary rocks; influence of provenance and sedimentary processes. Rev. Mineral. Geochem. 21, 169–200.

McLennan, S.M., Hemming, S., McDaniel, D.K., Hanson, G.N., 1993a. Geochemical approaches to sedimentation, provenance, and tectonics, in: Geological Society of America Special Papers. Geological Society of America, pp. 21–40. https://doi.org/10.1130/SPE284-p21

McLennan, S.M., Hemming, S., McDaniel, D.K., Hanson, G.N., 1993b. Geochemical approaches to sedimentation, provenance, and tectonics. Geol. Soc. Am. Spec. Pap. 284, 21–40. https://doi.org/10.1130/SPE284-p21

McReath, I., Faraco, M.T.L., 2005. Paleoproterozoic greenstone-granite belts in Northern Brazil and the former Guyana Shield - West African Craton province. Geol. USP Sér. Científica 5, 49–63. https://doi.org/10.5327/S1519-874X2006000100004

Mercier de Lépinay, M., Loncke, L., Basile, C., Roest, W.R., Patriat, M., Maillard, A., De Clarens, P., 2016. Transform continental margins – Part 2: A worldwide review. Tectonophysics 693, 96–115. https://doi.org/10.1016/j.tecto.2016.05.038

Meyers, P.A., 1997. Organic geochemical proxies of paleoceanographic, paleolimnologic, and paleoclimatic processes. Org. Geochem. 27, 213–250. https://doi.org/10.1016/S0146-6380(97)00049-1

Meyers, P.A., Bernasconi, S.M., Forster, A., 2006. Origins and accumulation of organic matter in expanded Albian to Santonian black shale sequences on the Demerara Rise, South American margin. Org. Geochem., Advances in Organic Geochemistry 2005 37, 1816–1830. https://doi.org/10.1016/j.orggeochem.2006.08.009

Min, A.D., Piccirillo, E.M., Marzoli, A., Bellieni, G., Renne, P.R., Ernesto, M., Marques, L.S., 2013. The Central Atlantic Magmatic Province (CAMP) in Brazil: Petrology, Geochemistry, 40Ar/39Ar Ages, Paleomagnetism and Geodynamic Implications, in: The Central Atlantic Magmatic Province: Insights from Fragments of Pangea. American Geophysical Union (AGU), pp. 91–128. https://doi.org/10.1029/136GM06

Moiroud, M., Pucéat, E., Donnadieu, Y., Bayon, G., Guiraud, M., Voigt, S., Deconinck, J.-F., Monna, F., 2016. Evolution of neodymium isotopic signature of seawater during the Late Cretaceous: Implications for intermediate and deep circulation. Gondwana Res. 36, 503–522. https://doi.org/10.1016/j.gr.2015.08.005

Monteiro, H.S., Vasconcelos, P.M.P., Farley, K.A., Lopes, C.A.M., 2018. Age and evolution of diachronous erosion surfaces in the Amazon: Combining (U-Th)/He and cosmogenic 3He records. Geochim. Cosmochim. Acta 229, 162–183. https://doi.org/10.1016/j.gca.2018.02.045

Montgomery, C.W., Hurley, P.M., 1978. Total-rock UPb and RbSr systematics in the Imataca Series, Guayana Shield, Venezuela. Earth Planet. Sci. Lett. 39, 281–290. https://doi.org/10.1016/0012-821X(78)90204-2

Moquet, J.-S., Morera, S., Turcq, B., Poitrasson, F., Roddaz, M., Moreira-Turcq, P., Espinoza, J.C., Guyot, J.-L., Takahashi, K., Orrillo-Vigo, J., Petrick, S., Mounic, S., Sondag, F., 2020. Control of seasonal and inter-annual rainfall distribution on the Strontium-Neodymium isotopic compositions of suspended particulate matter and implications for tracing ENSO events in the Pacific coast (Tumbes basin, Peru). Glob. Planet. Change 185, 103080. https://doi.org/10.1016/j.gloplacha.2019.103080

Morais Neto, J.M., Hegarty, K.A., Karner, G.D., Alkmim, F.F., 2009. Timing and mechanisms for the generation and modification of the anomalous topography of the Borborema Province, northeastern Brazil. Mar. Pet. Geol. 26, 1070–1086. https://doi.org/10.1016/j.marpetgeo.2008.07.002

Moreau, C., Ohnenstetter, D., Demaiffe, D., Robineau, B., 1996. The Los Archipelago nepheline syenite ring-structure: A magmatic marker of the evolution of the central and equatorial atlantic. Can. Mineral. 34, 281–299.

Moulin, M., Aslanian, D., Unternehr, P., 2010. A new starting point for the South and Equatorial Atlantic Ocean. Earth-Sci. Rev. 98, 1–37. https://doi.org/10.1016/j.earscirev.2009.08.001

Mourlot, Y., 2018. Contrôles sur la répartition des argiles organiques dans les bassins profonds : cas de l'Atlantique central au Crétacé (thesis). http://www.theses.fr. Toulouse 3.

Mourlot, Y., Roddaz, M., Dera, G., Calvès, G., Kim, J., Chaboureau, A., Mounic, S., Raisson, F., 2018a. Geochemical Evidence for Large- Scale Drainage Reorganization in Northwest Africa During the Cretaceous. Geochem. Geophys. Geosystems 0. https://doi.org/10.1029/2018GC007448

Mourlot, Y., Calvès, G., Clift, P.D., Baby, G., Chaboureau, A.-C., Raisson, F., 2018b. Seismic stratigraphy of Cretaceous eastern Central Atlantic Ocean: Basin evolution and

palaeoceanographic implications. Earth Planet. Sci. Lett. 499, 107–121. https://doi.org/10.1016/j.epsl.2018.07.023

Müller, R.D., Smith, W.H.F., 1993. Deformation of the oceanic crust between the North American and South American Plates. J. Geophys. Res. Solid Earth 98, 8275–8291. https://doi.org/10.1029/92JB02863

Nemčok, M., Rybár, S., Sinha, S.T., Hermeston, S.A., Ledvényiová, L., 2016. Transform margins: development, controls and petroleum systems – an introduction. Geol. Soc. Lond. Spec. Publ. 431, 1–38. https://doi.org/10.1144/SP431.15

Nesbitt, H.W., Young, G.M., 1982. Early Proterozoic climates and plate motions inferred from major element chemistry of lutites. Nature 299, 715–717. https://doi.org/10.1038/299715a0

Nesbitt, H.W., Young, G.M., McLennan, S.M., Keays, R.R., 1996. Effects of Chemical Weathering and Sorting on the Petrogenesis of Siliciclastic Sediments, with Implications for Provenance Studies. J. Geol. 104, 525–542. https://doi.org/10.1086/629850

Nixon, P.H., Davies, G.R., Rex, D.C., Gray, A., 1992. Venezuela kimberlites. J. Volcanol. Geotherm. Res. 50, 101–115. https://doi.org/10.1016/0377-0273(92)90039-G

Nogueira, S.A.A., Bettencourt, J.S., Tassinari, C.C.G., 2017. GEOCHRONOLOGY OF THE GRANITOID HOSTED SALAMANGONE GOLD DEPOSIT, LOURENÇO DISTRICT, AMAPÁ, BRAZIL. Rev. Bras. Geociências 30, 261–264.

Oliveira, E.C., Lafon, J.-M., Gioia, S.M.C.L., Pimentel, M.M., 2008. Datação Sm-Nd em rocha total e granada do metamorfismo granulítico da região de Tartarugal Grande, Amapá Central. Rev. Bras. Geociências 38, 114–127.

Olszewski, W.J., Wirth, K.R., Gibbs, A.K., Gaudette, H.E., 1989. The age, origin, and tectonics of the Grão Pará Group and associated rocks, Serra dos Carajás, Brazil: Archean continental volcanism and rifting. Precambrian Res., Precambrian Research Recent Advances of the Precambrain Geology of South and Central America and the Caribbean 42, 229–254. https://doi.org/10.1016/0301-9268(89)90013-2

Olyphant, J.R., Johnson, R.A., Hughes, A.N., 2017. Evolution of the Southern Guinea Plateau: Implications on Guinea-Demerara Plateau formation using insights from seismic, subsidence, and gravity data. Tectonophysics 717, 358–371. https://doi.org/10.1016/j.tecto.2017.08.036

Othman, D.B., Polvé, M., Allègre, C.J., 1984. Nd—Sr isotopic composition of granulites and constraints on the evolution of the lower continental crust. Nature 307, 510–515. https://doi.org/10.1038/307510a0

Palmer, M.R., Edmond, J.M., 1992. Controls over the strontium isotope composition of river water. Geochim. Cosmochim. Acta 56, 2099–2111. https://doi.org/10.1016/0016-7037(92)90332-D

Patchett, P.J., Ross, G.M., Gleason, J.D., 1999. Continental Drainage in North America During the Phanerozoic from Nd Isotopes. Science 283, 671–673. https://doi.org/10.1126/science.283.5402.671

Peulvast, J.-P., Bétard, F., 2015. A history of basin inversion, scarp retreat and shallow denudation: The Araripe basin as a keystone for understanding long-term landscape evolution in NE Brazil. Geomorphology, Patterns and rates of Cenozoic landscape change in orogenic and post-orogenic settings 233, 20–40. https://doi.org/10.1016/j.geomorph.2014.10.009

Pindell, J.L., 1991. Geologic Rationale for Hydrocarbon Exploration in the Caribbean and Adjacent Regions. J. Pet. Geol. 14, 237–258. https://doi.org/10.1111/j.1747-5457.1991.tb00310.x

Posadas, V.G., Kalliokoski, J., 1967. Rb-Sr ages of the encrucijada granite intrusive in the Imataca Complex, Venezuela. Earth Planet. Sci. Lett. 2, 210–214. https://doi.org/10.1016/0012-821X(67)90130-6

Potter, P.E., 1997. The Mesozoic and Cenozoic paleodrainage of South America: a natural history. J. South Am. Earth Sci. 10, 331–344. https://doi.org/10.1016/S0895-9811(97)00031-X

Pourmand, A., Dauphas, N., Ireland, T.J., 2012. A novel extraction chromatography and MC-ICP-MS technique for rapid analysis of REE, Sc and Y: Revising CI-chondrite and Post-Archean Australian Shale (PAAS) abundances. Chem. Geol. 291, 38–54. https://doi.org/10.1016/j.chemgeo.2011.08.011

Priem, H.N.A., Boelrijk, N. a. I.M., Hebeda, E.H., Verdurmen, E. a. T., Verschure, R.H., 1971. Isotopic Ages of the Trans-Amazonian Acidic Magmatism and the Nickerie Metamorphic Episode in the Precambrian Basement of Suriname, South America. GSA Bull. 82, 1667–1680. https://doi.org/10.1130/0016-7606(1971)82[1667:IAOTTA]2.0.CO;2

Priem, H.N.A., Boelrijk, N. a. I.M., Hebeda, E.H., Verdurmen, E.A.T., Verschure, R.H., 1973. Age of the Precambrian Roraima Formation in Northeastern South America: Evidence from Isotopic Dating of Roraima Pyroclastic Volcanic Rocks in Suriname. GSA Bull. 84, 1677–1684. https://doi.org/10.1130/0016-7606(1973)84<1677:AOTPRF>2.0.CO;2

Reis, N.J., Teixeira, W., Hamilton, M.A., Bispo-Santos, F., Almeida, M.E., D'Agrella-Filho, M.S., 2013. Avanavero mafic magmatism, a late Paleoproterozoic LIP in the Guiana

Shield, Amazonian Craton: U–Pb ID-TIMS baddeleyite, geochemical and paleomagnetic evidence. Lithos, Large Igneous Provinces (LIPs) and Supercontinents 174, 175–195. https://doi.org/10.1016/j.lithos.2012.10.014

Reuber, K.R., Pindell, J., Horn, B.W., 2016. Demerara Rise, offshore Suriname: Magma-rich segment of the Central Atlantic Ocean, and conjugate to the Bahamas hot spot. Interpretation 4, T141–T155. https://doi.org/10.1190/INT-2014-0246.1

Roddaz, M., Nauton-Fourteu, M., Santos, R.V., Dantas, E.L., Calves, G., 2020. Controls on the provenance of late Eocene to Quaternary Mozambique Channel shales (DSDP 25 Site 242). Mar. Geol. 421, 106090. https://doi.org/10.1016/j.margeo.2019.106090

Roddaz, M., Viers, J., Brusset, S., Baby, P., Boucayrand, C., Hérail, G., 2006. Controls on weathering and provenance in the Amazonian foreland basin: Insights from major and trace element geochemistry of Neogene Amazonian sediments. Chem. Geol. 226, 31–65. https://doi.org/10.1016/j.chemgeo.2005.08.010

Roddaz, M., Viers, J., Brusset, S., Baby, P., Hérail, G., 2005. Sediment provenances and drainage evolution of the Neogene Amazonian foreland basin. Earth Planet. Sci. Lett. 239, 57–78. https://doi.org/10.1016/j.epsl.2005.08.007

Roddaz, M., Viers, J., Moreira-Turcq, P., Blondel, C., Sondag, F., Guyot, J.-L., Moreira, L., 2014. Evidence for the control of the geochemistry of Amazonian floodplain sediments by stratification of suspended sediments in the Amazon. Chem. Geol. 387, 101–110. https://doi.org/10.1016/j.chemgeo.2014.07.022

Rousseau, T.C.C., Roddaz, M., Moquet, J.-S., Delgado, H.H., Calves, G., Bayon, G., 2019. Controls on the geochemistry of suspended sediments from large tropical South

American rivers (Amazon, Orinoco and Maroni). Chem. Geol. https://doi.org/10.1016/j.chemgeo.2019.05.027

Rousseau, T.C.C., Sonke, J.E., Chmeleff, J., Beek, P. van, Souhaut, M., Boaventura, G., Seyler, P., Jeandel, C., 2015. Rapid neodymium release to marine waters from lithogenic sediments in the Amazon estuary. Nat. Commun. 6, 1–8. https://doi.org/10.1038/ncomms8592

Santos, J.O.S., Hartmann, L.A., Gaudette, H.E., Groves, D.I., Mcnaughton, N.J., Fletcher, I.R., 2000. A New Understanding of the Provinces of the Amazon Craton Based on Integration of Field Mapping and U-Pb and Sm-Nd Geochronology. Gondwana Res. 3, 453–488. https://doi.org/10.1016/S1342-937X(05)70755-3

Santos, R.V., Sondag, F., Cochonneau, G., Lagane, C., Brunet, P., Hattingh, K., Chaves, J.G.S., 2015. Source area and seasonal 87Sr/86Sr variations in rivers of the Amazon basin. Hydrol. Process. 29, 187–197. https://doi.org/10.1002/hyp.10131

Sapin, F., Davaux, M., Dall'asta, M., Lahmi, M., Baudot, G., Ringenbach, J.-C., 2016. Post-rift subsidence of the French Guiana hyper-oblique margin: from rift-inherited subsidence to Amazon deposition effect. Geol. Soc. Lond. Spec. Publ. 431, 125–144. https://doi.org/10.1144/SP431.11

Sato, K., 1998. Evolução Crustal da Plataforma Sul Americana, com Base na Geoquímica Isotópica Sm-Nd (text). Universidade de São Paulo. https://doi.org/10.11606/T.44.1998.tde-29102012-144139

Schlanger, S.O., Jenkyns, H.C., 1976. Cretaceous Oceanic Anoxic Events: Causes and Consequences. Geol. En Mijnb. 55.

Schulte, P., Deutsch, A., Salge, T., Berndt, J., Kontny, A., MacLeod, K.G., Neuser, R.D., Krumm, S., 2009. A dual-layer Chicxulub ejecta sequence with shocked carbonates from the Cretaceous–Paleogene (K–Pg) boundary, Demerara Rise, western Atlantic. Geochim. Cosmochim. Acta 73, 1180–1204. https://doi.org/10.1016/j.gca.2008.11.011

Sibuet, J.-C., Mascle, J., 1978. Plate kinematic implications of Atlantic equatorial fracture zone trends. J. Geophys. Res. Solid Earth 83, 3401–3421. https://doi.org/10.1029/JB083iB07p03401

Souza, V. da S., Souza, A.G.H. de, Dantas, E.L., Valério, C. da S., Souza, V. da S., Souza, A.G.H. de, Dantas, E.L., Valério, C. da S., 2015. K'Mudku A-type magmatism in the southernmost Guyana Shield, central-north Amazon Craton (Brazil): the case of Pedra do Gavião syenogranite. Braz. J. Geol. 45, 293–306. https://doi.org/10.1590/23174889201500020008

Spooner, C.M., Berrangé, J.P., Fairbairn, H.W., 1971. Rb-Sr Whole-Rock Age of the Kanuku Complex, Guyana. GSA Bull. 82, 207–210. https://doi.org/10.1130/0016-7606(1971)82[207:RWAOTK]2.0.CO;2

Tassinari, C.C.G., 1981. Evolução geotectônica da província Rio Negro-Jurena na região amazônica (text). Universidade de São Paulo. https://doi.org/10.11606/D.44.1981.tde-11062013-163626

Tassinari, C.C.G., Munhá, J.M.U., Teixeira, W., Palácios, T., Nutman, A.P., S, C.S., Santos, A.P., Calado, and B.O., 2004. The Imataca Complex, NW Amazonian Craton, Venezuela: Crustal evolution and integration of geochronological and petrological cooling histories. Episodes J. Int. Geosci. 27, 3–12. https://doi.org/10.18814/epiiugs/2004/v27i1/002

Taylor, S.R., McLennan, S.M., 1985. The continental crust: Its composition and evolution.

Teixeira, W., Tassinari, C.C.G., Cordani, U.G., Kawashita, K., 1989. A review of the geochronology of the Amazonian Craton: Tectonic implications. Precambrian Res., Precambrian Research Recent Advances of the Precambrain Geology of South and Central America and the Caribbean 42, 213–227. https://doi.org/10.1016/0301-9268(89)90012-0

Tello Saenz, C.A., Hackspacher, P.C., Hadler Neto, J.C., Iunes, P.J., Guedes, S., Ribeiro, L.F.B., Paulo, S.R., 2003. Recognition of Cretaceous, Paleocene, and Neogene tectonic reactivation through apatite fission-track analysis in Precambrian areas of southeast Brazil: association with the opening of the south Atlantic Ocean. J. South Am. Earth Sci. 15, 765–774. https://doi.org/10.1016/S0895-9811(02)00131-1

Torsvik, T.H., Van der Voo, R., Preeden, U., Mac Niocaill, C., Steinberger, B., Doubrovine, P.V., van Hinsbergen, D.J.J., Domeier, M., Gaina, C., Tohver, E., Meert, J.G., McCausland, P.J.A., Cocks, L.R.M., 2012. Phanerozoic polar wander, palaeogeography and dynamics. Earth-Sci. Rev. 114, 325–368. https://doi.org/10.1016/j.earscirev.2012.06.007

Tyson, R., 1995. Sedimentary Organic Matter: Organic facies and palynofacies. Springer Netherlands. https://doi.org/10.1007/978-94-011-0739-6

Vanderhaeghe, O., Ledru, P., Thiéblemont, D., Egal, E., Cocherie, A., Tegyey, M., Milési, J.-P., 1998. Contrasting mechanism of crustal growth: Geodynamic evolution of the Paleoproterozoic granite–greenstone belts of French Guiana. Precambrian Res. 92, 165–193. https://doi.org/10.1016/S0301-9268(98)00074-6

Vermeesch, P., 2018. Statistical models for point-counting data. Earth Planet. Sci. Lett. 501, 112–118. https://doi.org/10.1016/j.epsl.2018.08.019

Vermeesch, P., 2004. How many grains are needed for a provenance study? Earth Planet. Sci. Lett. 224, 441–451. https://doi.org/10.1016/j.epsl.2004.05.037

Viers, J., Roddaz, M., Filizola, N., Guyot, J.-L., Sondag, F., Brunet, P., Zouiten, C., Boucayrand, C., Martin, F., Boaventura, G.R., 2008. Seasonal and provenance controls on Nd–Sr isotopic compositions of Amazon rivers suspended sediments and implications for Nd and Sr fluxes exported to the Atlantic Ocean. Earth Planet. Sci. Lett. 274, 511–523. https://doi.org/10.1016/j.epsl.2008.08.011

Voicu, G., Bardoux, M., Stevenson, R., Jébrak, M., 2000. Nd and Sr isotope study of hydrothermal scheelite and host rocks at Omai, Guiana Shield: implications for ore fluid source and flow path during the formation of orogenic gold deposits. Miner. Deposita 35, 302–314. https://doi.org/10.1007/s001260050243

Weltje, G.J., 2012. Quantitative models of sediment generation and provenance: State of the art and future developments. Sediment. Geol., Actualistic Models of Sediment Generation 280, 4–20. https://doi.org/10.1016/j.sedgeo.2012.03.010

White, W.M., Dupré, B., Vidal, P., 1985. Isotope and trace element geochemistry of sediments from the Barbados Ridge-Demerara Plain region, Atlantic Ocean. Geochim. Cosmochim. Acta 49, 1875–1886. https://doi.org/10.1016/0016-7037(85)90082-1

Yang, W., Escalona, A., 2011. Tectonostratigraphic evolution of the Guyana Basin. AAPG Bull. 95, 1339–1368. https://doi.org/10.1306/01031110106

Figure captions

Figure 1. A) Location of study area in its Cretaceous paleogeographical context (Torsvik et al., 2012). The red rectangle indicates position of area shown on Figure 1B. WAC: West African Craton. B) Map of the Precambrian Guiana Shield, Mesozoic Takutu basin (TkB), and location of studied Arapaima-1 well (AR-1, red circle)

Figure 2. Stratigraphy and sedimentary log section of Arapaima-1 well including $\delta^{13}C_{TOC}$ data, TOC contents, sedimentation rate and main geodynamic events at the scale of Guyana-Suriname basin. The stratigraphic position of analyzed samples is indicated by orange triangle. AR-1: Arapaima-1 well. M: mudstone. W: wackestone. P: packstone. G: grainstone. C: clay. S: silt. FS: fine sandstone. MS: medium sandstone. CS: coarse sandstone. Details on the calculation of sedimentation rates can be found in (Mourlot, 2018). References for timing and duration of main geodynamic events are as follow : South Atlantic Ocean opening (Hall et al., 2018), Equatorial Atlantic Ocean opening (Moulin et al., 2010; Sibuet and Mascle, 1978), Albian-Coniacian cooling (Benkhelil et al., 1995; Yang and Escalona, 2011), Central Atlantic spreading rate acceleration (Larson, 1991), Caribbean Large Igneous Province (Loewen et al., 2013), Andean deformation (Hurtado et al., 2018; Louterbach et al., 2018).

Figure 3. Map showing the main geological units of the Guiana Shield (simplified from (Kroonenberg et al., 2016)) and the localization of the main northern South American rivers. Mean values for $\varepsilon_{Nd(0)}$ and $^{87}Sr/^{86}Sr$ isotopic composition of the main geological unit of the Guiana Shield are given (See Table 1 and text for details and references).

Figure 4. Major and selected trace element contents of analyzed samples normalized to PAAS (Pourmand et al., 2012; Taylor and McLennan, 1985). From left to right on the diagram, these

include the major elements (SiO_2, TiO_2, Al_2O_3, Fe_2O_3, MnO, MgO, CaO, Na_2O, K_2O and P_2O_5), LILE (Rb, Cs, Ba, Sr, Th and U), HFSE (Y, Zr, Nb, Hf), and TTE (Sc, Cr, Co, V and Ni).

Figure 5. Rare earth element (REE) contents of studied samples normalized to PAAS (Pourmand et al., 2012; Taylor and McLennan, 1985).

Figure 6. Stratigraphic variation of Nd and Sr isotope compositions (expressed as $\varepsilon_{Nd(0)}$ and $^{87}Sr/^{86}Sr$) and selected trace element ratios (Cr/Th, Th/Sc and Eu/Eu*, see text for details) of analyzed samples. The lengths of the horizontal bar for the Sr-Nd isotopic compositions correspond to 1σ analytical errors (see Table 4). The horizontal bars for the Cr/Th, Th/Sc, and Eu/Eu* ratios correspond to 15% (i.e., the sum of the Cr and Th concentration analytical errors), 25% (i.e., the sum of the Th and Sc concentration analytical errors) and 5% (i.e., the Eu concentration analytical error, see supplementary material Table S2). Dashed lines in Eu/Eu*, Th/Sc and Cr/Th show the PAAS ratio values (Taylor and McLennan, 1985; Pourmand et al., 2012). Red and blue rectangles indicate the values range for felsic and basic sediments, respectively (Cullers, 2000).

Figure 7. HREE/LREE vs. MREE/MREE* diagram. HREE/LREE and MREE/MREE* values are calculated following (Martin et al., 2010) where HREE=Tm+Yb+Lu, LREE=La+Pr+Nd, MREE=Gd+Tb+Dy (all PAAS normalized), and MREE*=the average of HREE+LREE. The MREE bulge and "bell-shaped" REE profiles correspond to REE patterns observed in fish teeth, Fe-Mn oxides, organic matter and pore waters, while "HREE-enriched" profiles correspond to modern sea water (Huck et al., 2016; Moiroud et al., 2016). These end-members reflect the REE contents of marine sediments influenced by seawater or authigenic phases, while "flat" REE

patterns are characteristic of continental clays (see Huck et al., 2016; Moiroud et al., 2016 for a review). Analyzed samples are represented by specific symbols used in Figs 4 and 5.

Figure 8. Cross-plots of $\varepsilon_{Nd(0)}$ and $^{87}Sr/^{86}Sr$ values for the analyzed samples. The isotopic fields of potential end-members of the Guiana Shield are based on a compilation of published data (see Table 1 and supporting Table S1). AAIG: Archean granitoids (AAIG) (Barreto et al., 2013; da Rosa-Costa et al., 2006; Hurley et al., 1968; Montgomery and Hurley, 1978; Oliveira et al., 2008; Olszewski et al., 1989; Othman et al., 1984; Posadas and Kalliokoski, 1967; Tassinari et al., 2004) (Avelar et al. (2003); PGGF: Paleoproterozoic granitoids and felsic series (Barreto et al., 2013; Boher et al., 1992; da Rosa-Costa et al., 2006; Gaudette et al., 1978; Gruau et al., 1985; Hurley et al., 1968; Lenharo et al., 2002; Marques et al., 2014; McReath and Faraco, 2005; Nogueira et al., 2000; Priem et al., 1973, 1971; Sato, 1998; Tassinari, 1981; Voicu et al., 2000), Macambira et al. (1987) Jorge Joao et al. (1985), Gibbs and Barron (1993 Avelar et al. (2003); PHGB: Paleoproterozoic high-grade belt (Gaudette et al., 1996; Heinonen et al., 2012; Klaver et al., 2015; Othman et al., 1984; Sato, 1998; Spooner et al., 1971; Tassinari, 1981) de Roever et al. (2003) ; MG : Mesoproterozoic granitoids (Heinonen et al., 2012; Souza et al., 2015; Tassinari, 1981); PMI-GB: Paleoproterozoic mafic intrusions and greenstone belt (Gibbs et al., 1986; Gruau et al., 1985; Hebeda et al., 1973; Kaminsky et al., 2004; Leal et al., 2006; McReath and Faraco, 2005; Nixon et al., 1992; Santos et al., 2000; Sato, 1998; Voicu et al., 2000); JMD: Jurassic mafic dykes (Deckart et al., 2005; Min et al., 2013). To avoid outlier effects and important overlapping, the limits of each rectangular field are defined as the first quartile and the third quartile for each subset. Comparative clay data from the Demerara Rise and Demerara abyssal plain are added (Martin et al., 2012; Schulte et al., 2009; White et al., 1985). Sr-Nd isotopic compositions of suspended particulate matter and dissolved Sr transported by the main

tropical rivers of the northeastern part of South America (i.e., Amazon, lower and upper Orinoco, Rio Negro, Maroni, Trombetas, Caroni) (Allègre et al., 1996; Goldstein et al., 1997; Palmer and Edmond, 1992; Rousseau et al., 2019; Santos et al., 2015)are added. Note that, when unavailable, sediment $^{87}Sr/^{86}Sr$ values of rivers were replaced by water $^{87}Sr/^{86}Sr$ values.

Figure 9. Paleogeographic map at 90 Ma (modified from Scotese and Golonka (1997) showing potential provenance areas for the Guyana-Suriname basin for pre-Coniacian (in red dashed curve) and post-Coniacian (blue dashed curve) times. TkB: Takutu basin. AR-1: Arapaima-1 well.

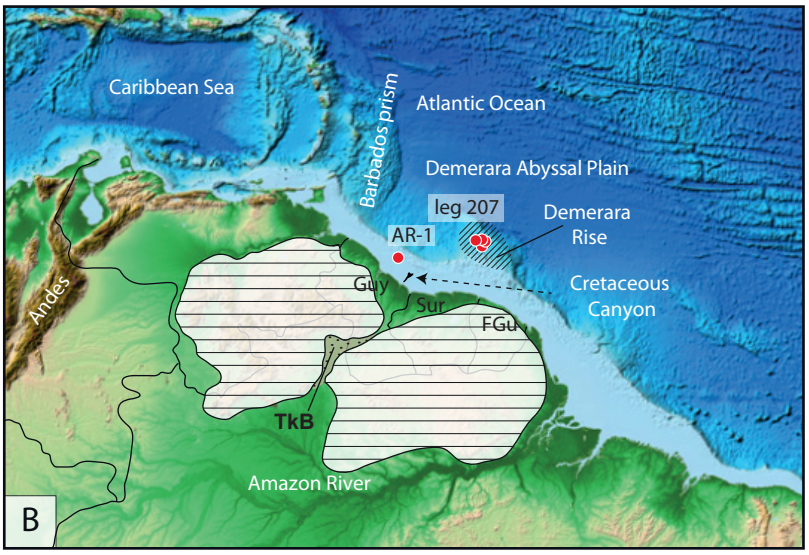

Precambrian Guiana Shield

Mesozoic sedimentary basin

Continent

Shallow marine

Deep marine

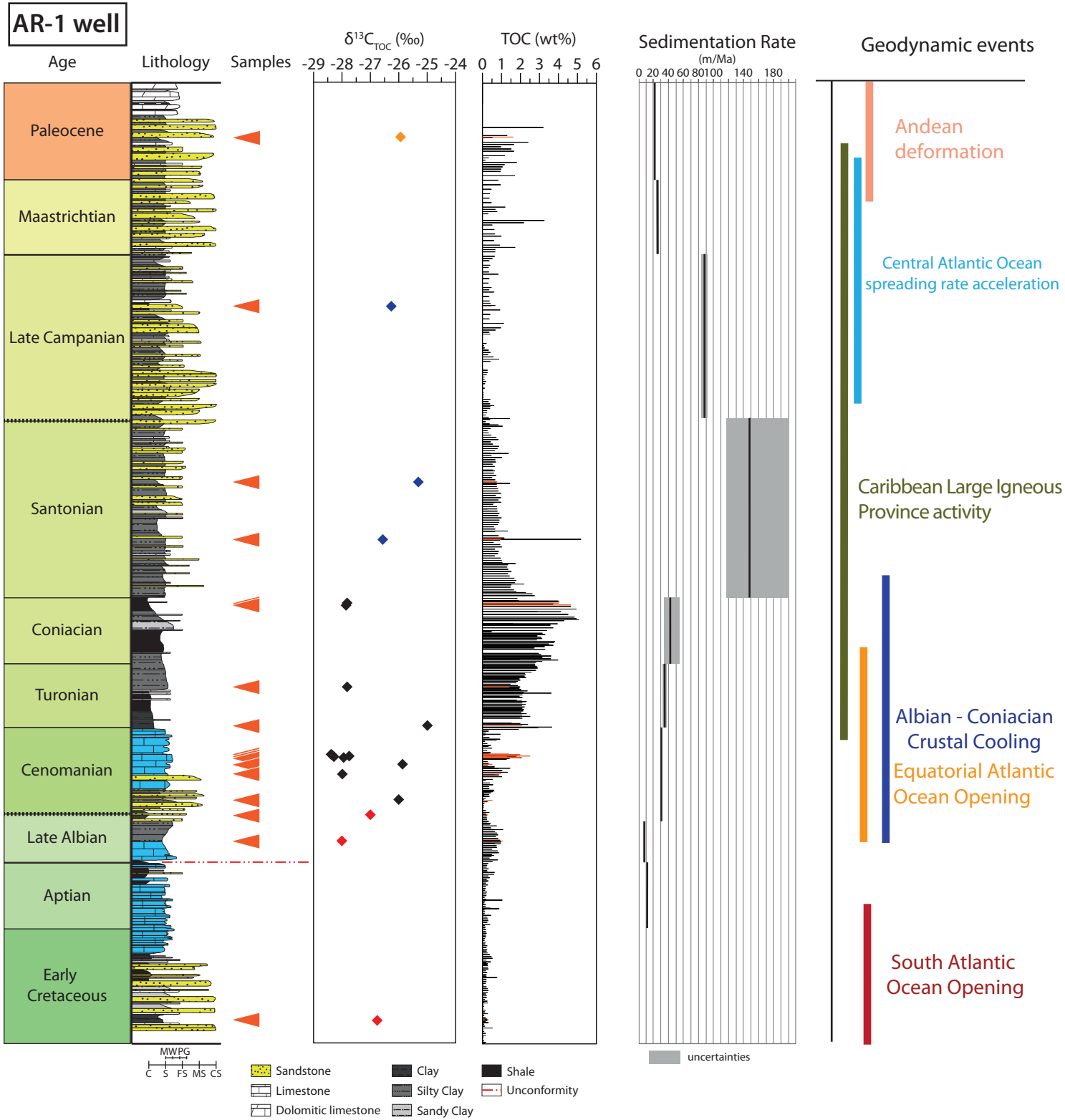
AR-1 well
Age
Lithology
Samples
δ13C TOC (‰)
-29 -28 -27 -26 -25 -24
TOC (wt%)
0 1 2 3 4 5 6
Sedimentation Rate
(m/Ma)
0 20 40 60 80 100 140 180
Geodynamic events
Paleocene
Maastrichtian
Late Campanian
Santonian
Coniacian
Turonian
Cenomanian
Late Albian
Aptian
Early Cretaceous
Andean deformation
Central Atlantic Ocean spreading rate acceleration
Caribbean Large Igneous Province activity
Albian - Coniacian Crustal Cooling
Equatorial Atlantic Ocean Opening
South Atlantic Ocean Opening
uncertainties
MWPG
C S FS MS CS
Sandstone
Limestone
Dolomitic limestone
Clay
Silty Clay
Sandy Clay
Shale
Unconformity

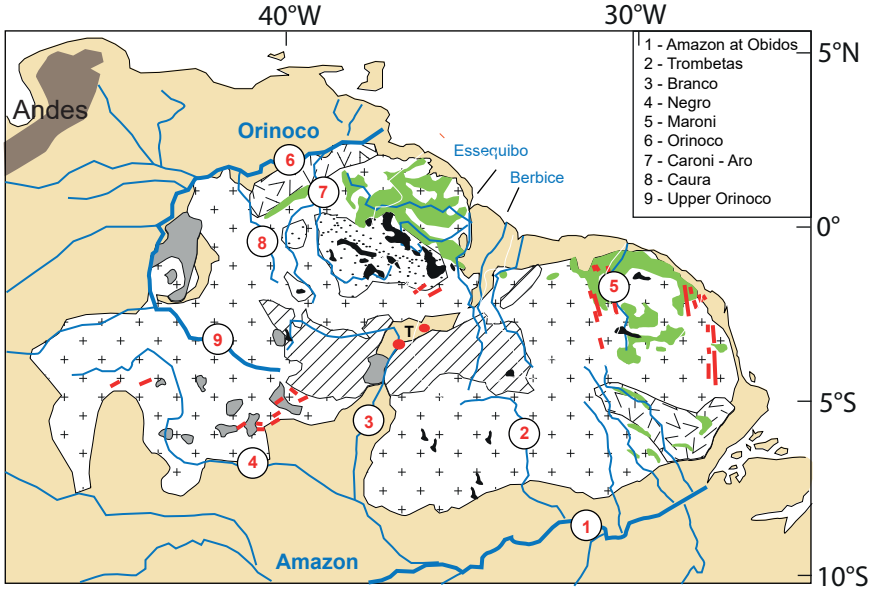

Felsic to intermediate sources:

AAIG - Archean Amapa & Imataca granitoids ($\varepsilon_{Nd(0)}$=-31.4 $^{87}Sr/^{86}Sr$=0.79509)

PGGF - Paleoproterozoic granitoids, gneiss & felsic volcanism ($\varepsilon_{Nd(0)}$=-23.4 $^{87}Sr/^{86}Sr$=0.77395)

PHGB - Paleoproterozoic high-grade granulite belts ($\varepsilon_{Nd(0)}$=-21.2 $^{87}Sr/^{86}Sr$=0.72025)

PRS - Paleoproterozoic Roraima sandstones

MG - Mesoproterozoic granites ($\varepsilon_{Nd(0)}$=-18.5 $^{87}Sr/^{86}Sr$=0.77460)

Mafic to utramafic sources:

GB - Greenstone Belt (metavolcanic) ($\varepsilon_{Nd(0)}$=-8.9 $^{87}Sr/^{86}Sr$=0.71051)

PMI - Precambrian mafic intrusions ($\varepsilon_{Nd(0)}$=-8.9 $^{87}Sr/^{86}Sr$=0.71051)

JMD - Jurassic mafic dykes ($\varepsilon_{Nd(0)}$=-0.2 $^{87}Sr/^{86}Sr$=0.70647)

Phanerozoic sedimentary cover

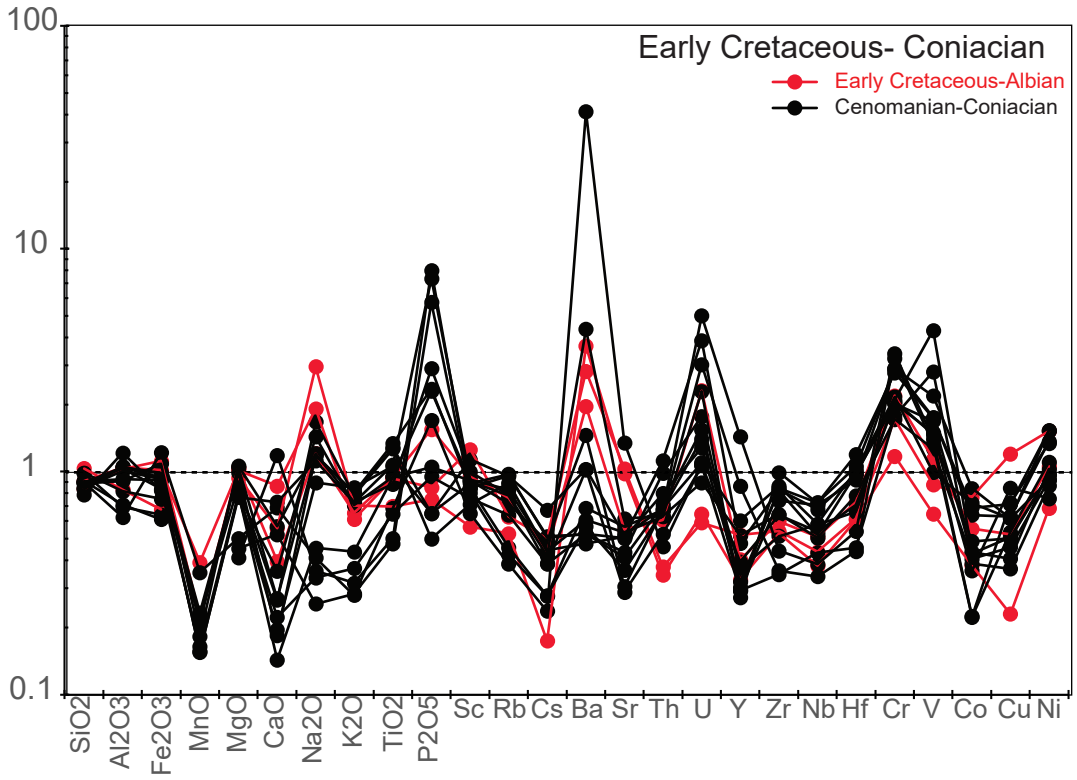
Early Cretaceous- Coniacian
Early Cretaceous-Albian
Cenomanian-Coniacian
100
10
1
0.1
SiO2
Al2O3
Fe2O3
MnO
MgO
CaO
Na2O
K2O
TiO2
P2O5
Sc
Rb
Cs
Ba
Sr
Th
U
Y
Zr
Nb
Hf
Cr
V
Co
Cu
Ni

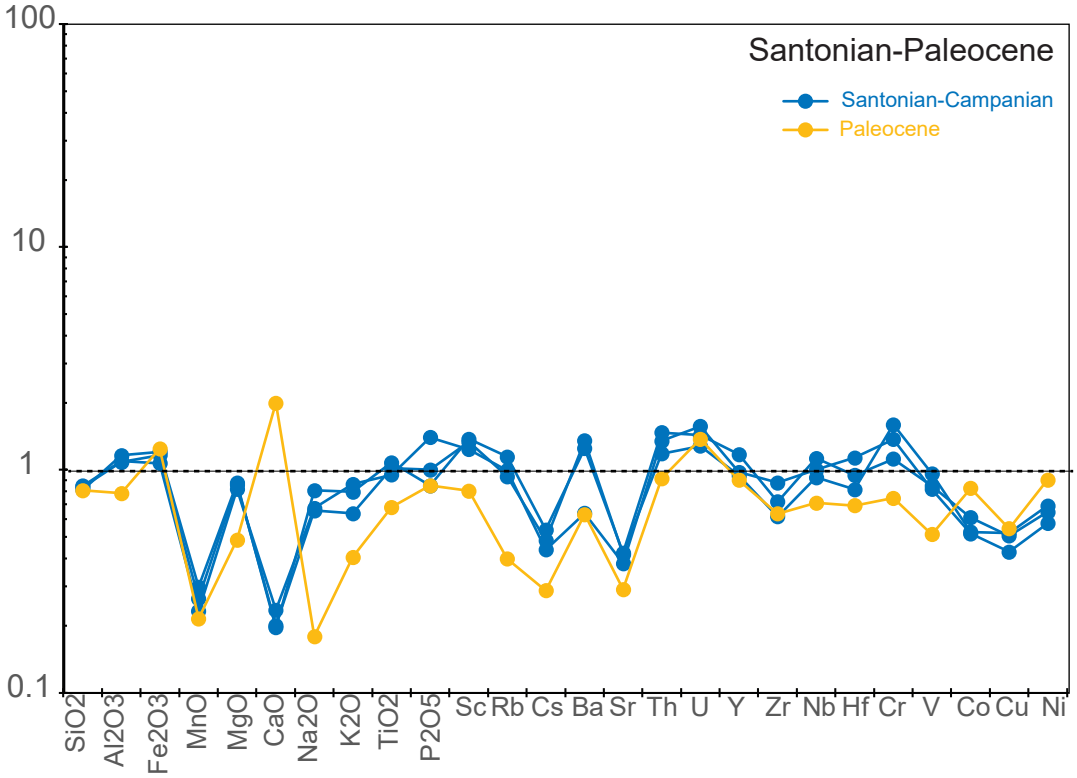
Santonian-Paleocene
Santonian-Campanian
Paleocene
100
10
1
0.1
SiO2
Al2O3
Fe2O3
MnO
MgO
CaO
Na2O
K2O
TiO2
P2O5
Sc
Rb
Cs
Ba
Sr
Th
U
Y
Zr
Nb
Hf
Cr
V
Co
Cu
Ni

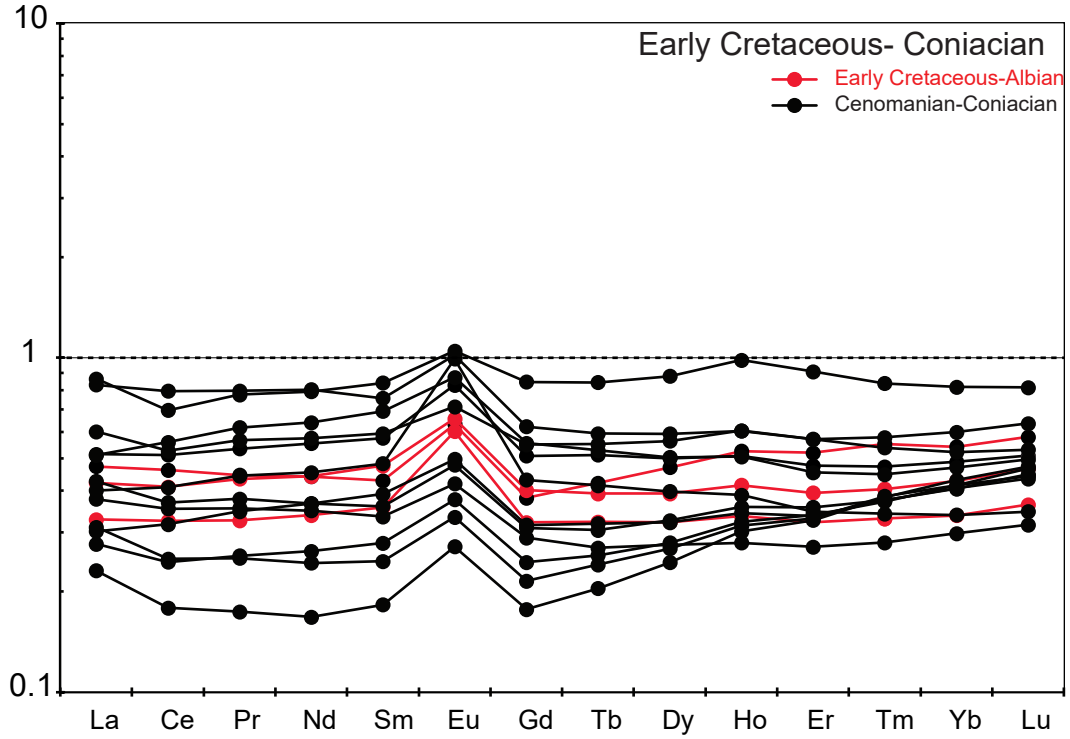
Early Cretaceous- Coniacian
Early Cretaceous-Albian
Cenomanian-Coniacian
10
1
0.1
La
Ce
Pr
Nd
Sm
Eu
Gd
Tb
Dy
Ho
Er
Tm
Yb
Lu

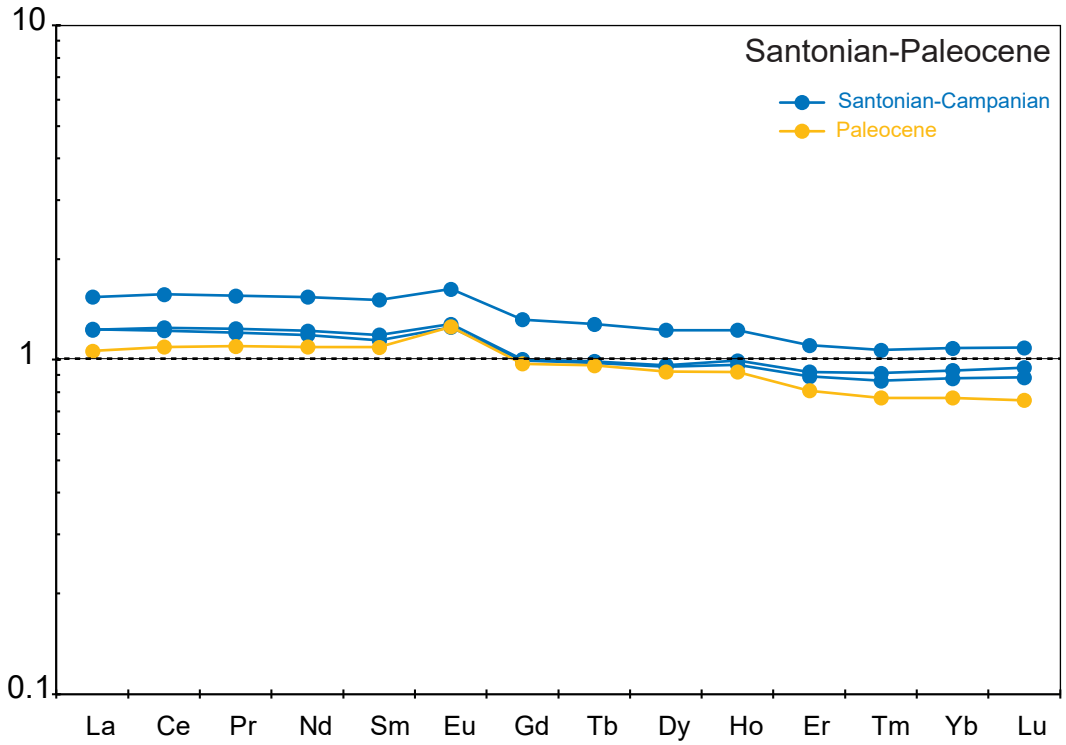
Santonian-Paleocene
Santonian-Campanian
Paleocene
10
1
0.1
La
Ce
Pr
Nd
Sm
Eu
Gd
Tb
Dy
Ho
Er
Tm
Yb
Lu

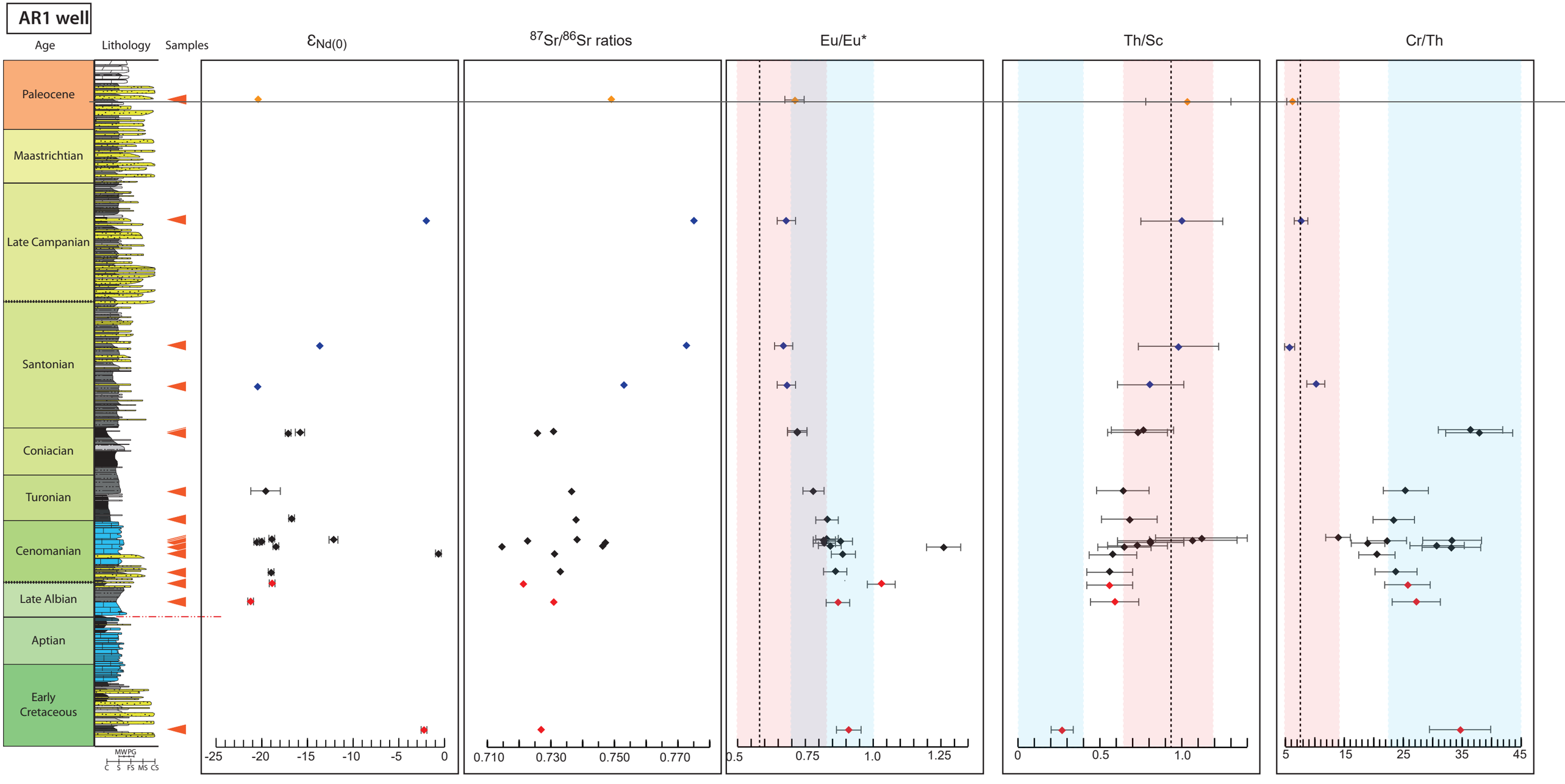
AR1 well
Age
Lithology
Samples
εNd(0)
87Sr/86Sr ratios
Eu/Eu*
Th/Sc
Cr/Th
Paleocene
Maastrichtian
Late Campanian
Santonian
Coniacian
Turonian
Cenomanian
Late Albian
Aptian
Early Cretaceous
MWPG
C S FS MS CS
-25 -20 -15 -10 -5 0
0.710 0.730 0.750 0.770
0.5 0.75 1.0 1.25
0 0.5 1.0
5 15 25 35 45

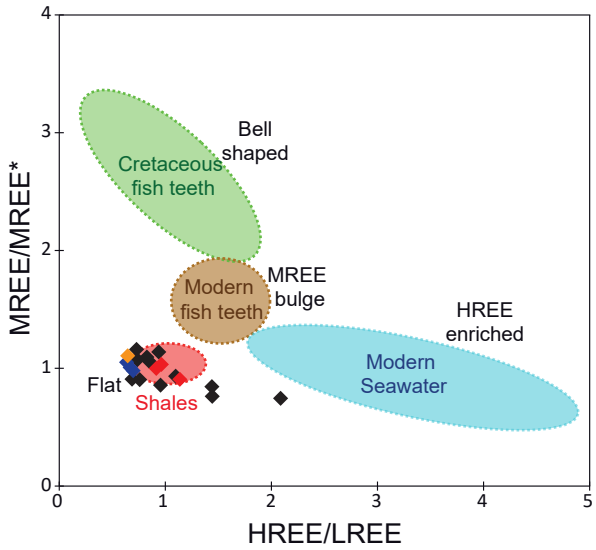
MREE/MREE*
HREE/LREE
0
1
2
3
4
5
Bell
shaped
Cretaceous
fish teeth
Modern
fish teeth
MREE
bulge
HREE
enriched
Modern
Seawater
Flat
Shales

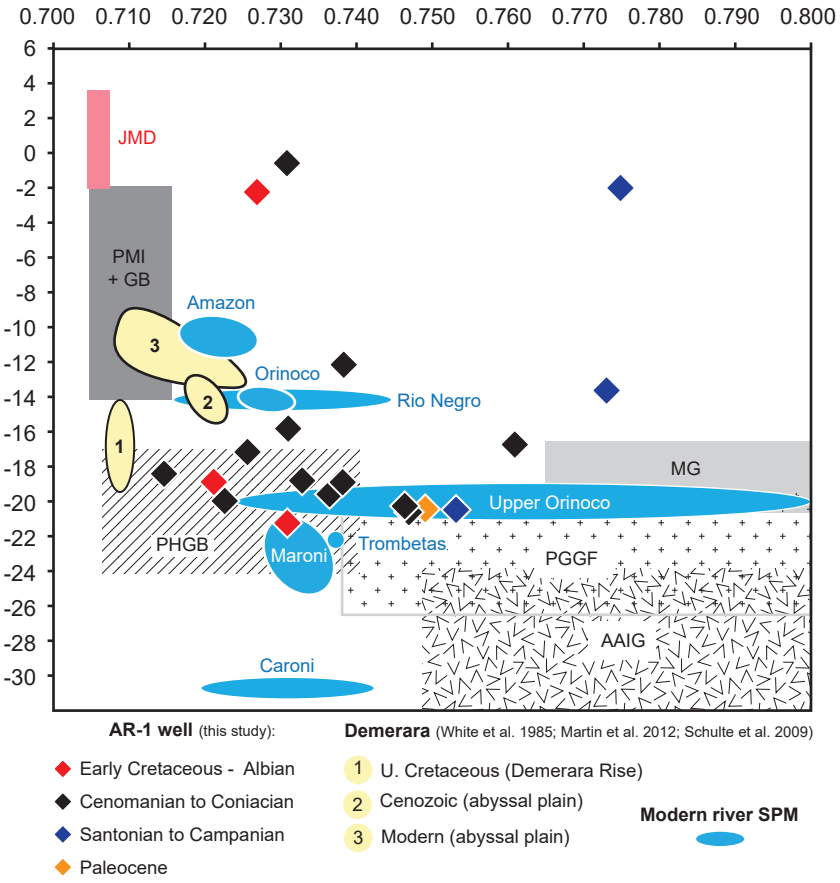
0.700
0.710
0.720
0.730
0.740
0.750
0.760
0.770
0.780
0.790
0.800
6
4
2
0
-2
-4
-6
-8
-10
-12
-14
-16
-18
-20
-22
-24
-26
-28
-30
JMD
PMI
+ GB
Amazon
3
Orinoco
2
Rio Negro
1
MG
Upper Orinoco
PHGB
Maroni
Trombetas
PGGF
AAIG
Caroni
AR-1 well (this study):
Early Cretaceous - Albian
Cenomanian to Coniacian
Santonian to Campanian
Paleocene
Demerara (White et al. 1985; Martin et al. 2012; Schulte et al. 2009)
1 U. Cretaceous (Demerara Rise)
2 Cenozoic (abyssal plain)
3 Modern (abyssal plain)
Modern river SPM

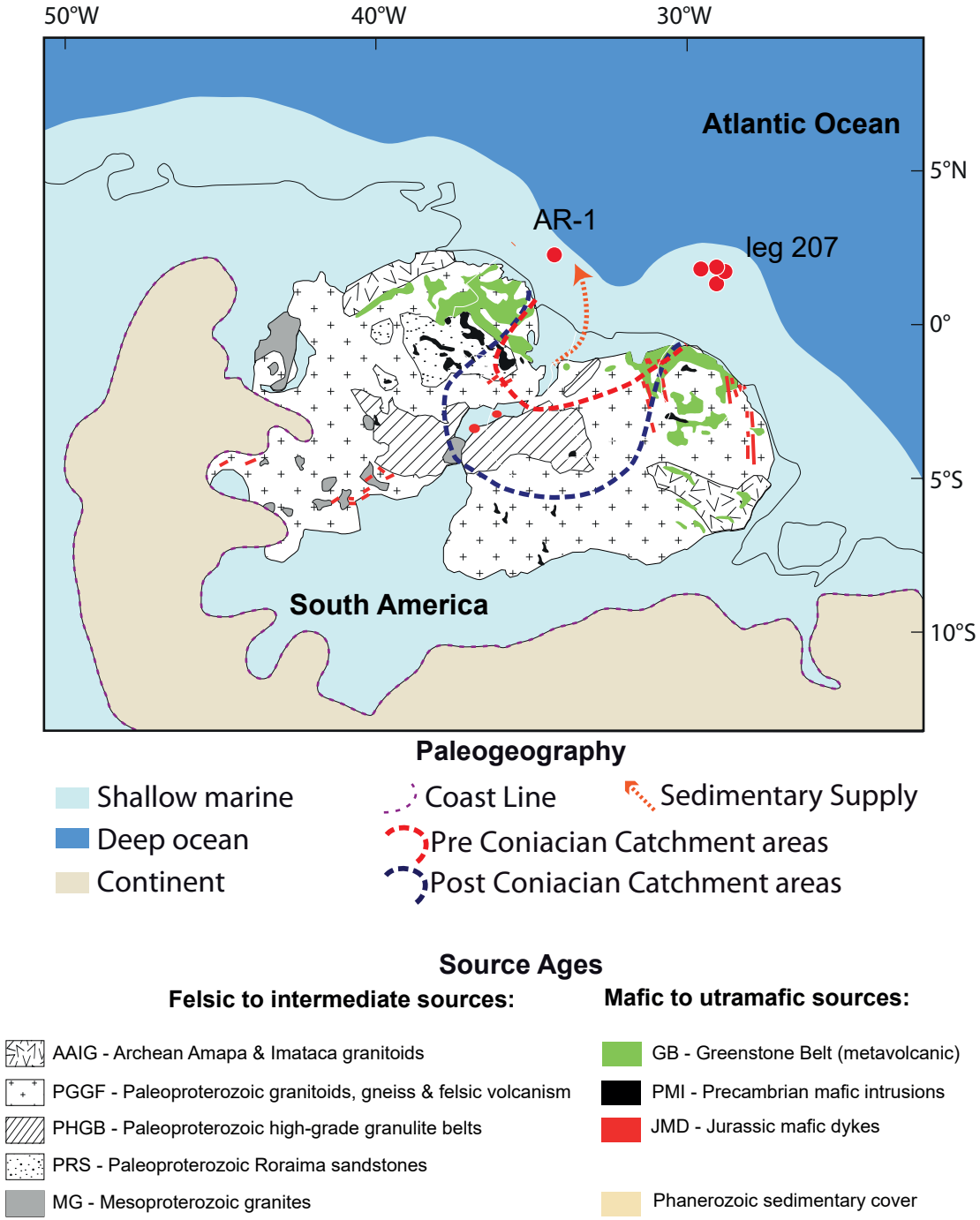
50°W
40°W
30°W
Atlantic Ocean
5°N
AR-1
leg 207
0°
5°S
South America
10°S
Paleogeography
Shallow marine
Deep ocean
Continent
Coast Line
Sedimentary Supply
Pre Coniacian Catchment areas
Post Coniacian Catchment areas
Source Ages
Felsic to intermediate sources:
AAIG - Archean Amapa & Imataca granitoids
PGGF - Paleoproterozoic granitoids, gneiss & felsic volcanism
PHGB - Paleoproterozoic high-grade granulite belts
PRS - Paleoproterozoic Roraima sandstones
MG - Mesoproterozoic granites
Mafic to utramafic sources:
GB - Greenstone Belt (metavolcanic)
PMI - Precambrian mafic intrusions
JMD - Jurassic mafic dykes
Phanerozoic sedimentary cover

$\varepsilon_{Nd(0)}$	AAIG	PGGF	PMI+GB	MG	PHGB	JMD
N	59	93	32	8	31	43
Min	-42.8	-42.8	-19.3	-21.2	-36.4	-4.6
Max	-1.9	-11.4	4.1	-15.3	-2.1	5.7
Mean	-30.2	-23.9	-7.8	-18.3	-20.4	0.4
Std. error	1.2	0.6	1.2	0.8	1.4	0.5
Variance	86.5	38.2	49.9	4.5	64.5	9.4
Stand. dev	9.3	6.2	7.1	2.1	8.0	3.1
Median	-31.4	-23.4	-8.9	-18.5	-21.2	-0.2
25 prcntil	-37.1	-26.6	-14.2	-20.5	-24.1	-2.1
75 prcntil	-23.9	-19.5	-1.9	-16.5	-17.1	3.6

$^{87}Sr/^{86}Sr$	AAIG	PGGF	PMI+GB	MG	PHGB	JMD
N	52	214	26	5	40	51
Min	0.70857	0.7015	0.704448	0.7645	0.7012	0.70292
Max	2.7365	4.4008	0.72945	0.8804	1.58175	0.711148
Mean	0.8880397	0.9097801	0.7111302	0.80524	0.7598767	0.706221
Std. error	0.0465425	0.0317048	0.0013489	0.023468	0.0248467	0.000237
Variance	0.1126428	0.2151119	4.73E-05	0.0027537	0.0246944	2.87E-06
Stand. dev	0.335623	0.4638016	0.0068782	0.0524761	0.1571444	0.0016928
Median	0.795095	0.77395	0.71051	0.7746	0.72025	0.70647
25 prcntil	0.7489525	0.738245	0.7048952	0.76535	0.7065225	0.70462
75 prcntil	0.838575	0.875025	0.7157525	0.86045	0.7402675	0.70746

Table 1: Mean εNd(0) values and 87Sr/86Sr isotopic composition and statistical parameters for potential end members; N: number of samples analyzed
Std error: Standard error; Stand. Dev: Standard deviation; 25 prcntil: first quartile; 75 prcntil: third quartile;
AAIG: Archean granitoid ; PGGF: Paleoproterozoic granitoids and felsic series; PMI+GB: Paleoproterozoic mafic intrusions and greenstone belt;
PHGB: Paleoproterozoic high-grade belt; MG: Mesoproterozoic granitoids; JMD: Jurassic Mafic Dykes
Data references:
AAIG: Barreto et al., 2013; da Rosa-Costa et al., 2006; Hurley et al., 1968; Montgomery and Hurley, 1978; Oliveira et al., 2008; Olszewski et al., 1989; Othman et al., 1984; Posadas and Kalliokoski, 1967; Tassinari et al., 2004) (Avelar et al. (2003); PGGF: Paleoproterozoic granitoids and felsic series (Barreto et al., 2013; Boher et al., 1992; da Rosa-Costa et al., 2006; Gaudette et al., 1978; Gruau et al., 1985; Hurley et al., 1968; Lenharo et al., 2002; Marques et al., 2014; McReath and Faraco, 2005; Nogueira et al., 2000; Priem et al., 1973, 1971; Sato, 1998; Tassinari, 1981; Voicu et al., 2000), Macambira et al. (1987) Jorge Joao et al. (1985), Gibbs and Barron (1993 Avelar et al. (2003); PHGB: Paleoproterozoic high-grade belt (Gaudette et al., 1996; Heinonen et al., 2012; Klaver et al., 2015; Othman et al., 1984; Sato, 1998; Spooner et al., 1971; Tassinari, 1981) de Roever et al. (2003) ; MG : Mesoproterozoic granitoids (Heinonen et al., 2012; Souza et al., 2015; Tassinari, 1981); PMI-GB: Paleoproterozoic mafic intrusions and greenstone belt (Gibbs et al., 1986; Gruau et al., 1985; Hebeda et al., 1973; Kaminsky et al., 2004; Leal et al., 2006; McReath and Faraco, 2005; Nixon et al., 1992; Santos et al., 2000; Sato, 1998; Voicu et al., 2000); JMD: Jurassic mafic dykes (Deckart et al., 2005; De Min et al., 2003)

Sample	Age	$\delta^{13}C_{TOC}$ (‰ VPDB)	TOC (wt%)
AR1-1	Early Cretaceous	-26.7	0.2
AR1-6	Aptian	-28.0	1.1
AR1-7	Late Albian	-27.0	0.3
AR1-8	Late Albian	-26.1	0.5
AR1-9	Cenomanian	-28.0	1.0
AR1-10	Cenomanian	-25.8	0.5
AR1-11B	Cenomanian	-27.9	2.0
AR1-11C	Cenomanian	-28.3	1.3
AR1-11D	Cenomanian	-27.7	2.5
AR1-11E	Cenomanian	-28.4	1.9
AR1-11F	Cenomanian	-28.4	1.4
AR1-12A	Early Turonian	-25.0	2.1
AR1-14	Turonian	-27.9	1.6
AR1-17A	Coniacian	-28.0	4.6
AR1-17B	Coniacian	-27.8	4.0
AR1-20	Late Santonian	-26.6	1.0
AR1-21	Santonian?	-25.4	0.7
AR1-23	Late Campanian	-26.3	0.4
AR1-24	Paleocene	-25.9	1.6

Table 2 : Organic Matter Contents and Stable Carbon Isotope Values (TOC and δ13CTOC) of SedimentaryRocks Analysed in this Study

.

Sample	AR1-1	AR1-6	AR1-7	AR1-8	AR1-9	AR1-10	AR1-11B	AR1-11C	AR1-11D
Age	Early Cretaceous	Late Albian	Late Albian	Cenomanian	Cenomanian	Cenomanian	Cenomanian	Cenomanian	Cenomanian
wt%									
SiO_2	57.09	52.54	64.90	55.92	55.48	56.28	53.10	56.19	56.59
Al_2O_3	19.72	19.43	15.71	19.78	17.17	11.80	19.78	19.54	17.54
Fe_2O_3	6.60	7.25	4.40	6.05	7.06	7.92	6.43	5.44	5.94
MnO	0.04	0.02	< D.L.	0.02	0.02	0.04	0.02	0.02	0.02
MgO	2.23	2.28	2.06	1.72	2.34	1.11	2.18	1.74	1.91
CaO	1.12	0.52	0.73	0.25	0.74	0.90	0.24	0.47	0.35
Na_2O	2.30	1.45	3.55	1.07	1.45	0.49	1.42	1.72	2.01
K_2O	2.27	2.42	2.61	3.14	2.70	1.03	2.96	2.62	2.89
TiO_2	0.93	0.94	0.70	1.06	0.88	0.69	1.28	0.95	1.27
P_2O_5	0.17	0.31	0.15	0.13	0.58	0.34	0.13	0.46	0.10
LOI	7.67	12.71	5.46	10.91	11.46	16.75	12.79	11.28	10.76
Total	100.13	99.86	100.27	100.04	99.86	97.34	100.33	100.42	99.37
Al/Si	0.39	0.42	0.27	0.4	0.35	0.24	0.42	0.39	0.35
CIA	70	77	61	78	72	77	77	75	71
ppm									
Sc	19.99	15.09	8.99	18.03	15.86	10.32	14.11	14.38	11.36
Rb	100.58	122.28	84.48	152.45	125.62	61.58	155.82	125.04	142.04
Cs	7.49	6.53	2.61	10.10	6.27	3.56	7.58	5.77	6.57
Ba	1836.12	1277.34	2383.46	666.73	2829.03	26793.14	342.00	341.76	394.32
Sr	206.01	109.76	195.54	103.58	123.21	269.75	82.50	100.41	106.65
Th	5.45	8.86	5.02	10.01	9.21	6.74	10.36	11.67	9.20
U	1.83	7.15	2.01	3.40	2.77	3.34	4.78	3.96	7.11
Y	14.2	11.0	9.0	16.5	14.1	10.8	8.0	8.8	7.4
Zr	113.51	125.81	111.17	180.52	135.19	134.04	155.75	172.29	208.16
Nb	8.31	9.68	7.19	11.07	9.59	10.24	13.45	9.91	13.72
Hf	3.08	3.65	3.04	5.06	3.90	3.53	4.59	4.88	5.96
Cr	188.87	241.18	129.11	237.96	189.08	223.43	318.57	222.02	306.20
V	131.11	170.71	96.99	149.10	189.91	224.00	328.04	253.35	261.33
Co	17.68	12.74	8.74	16.64	9.34	8.26	19.35	9.87	15.84
Cu	59.98	26.15	11.49	30.82	22.90	42.30	30.89	25.37	35.73
Ni	83.74	58.08	37.68	50.53	50.53	41.69	84.40	53.40	83.96
Zn	75.66	97.99	53.24	54.71	103.01	89.60	92.53	142.13	114.22
La	21.07	18.82	14.63	36.97	22.94	17.86	13.87	13.48	10.28
Ce	40.70	36.29	28.68	70.13	45.19	36.16	22.10	28.02	15.76
Pr	4.53	4.41	3.31	8.08	5.43	4.50	2.55	3.53	1.77
Nd	16.46	16.49	12.62	29.99	20.68	16.94	9.08	13.69	6.25
Sm	2.95	3.27	2.46	5.20	3.96	3.32	1.69	2.69	1.26
Eu	0.77	0.80	0.73	1.24	1.01	1.21	0.41	0.61	0.33
Gd	2.30	2.43	1.94	3.76	3.07	2.60	1.30	1.91	1.07
Tb	0.38	0.35	0.29	0.53	0.46	0.37	0.21	0.28	0.18
Dy	2.50	2.09	1.72	3.16	2.67	2.12	1.43	1.72	1.30
Ho	0.55	0.44	0.35	0.63	0.53	0.41	0.33	0.36	0.32
Er	1.60	1.21	0.99	1.76	1.46	1.07	1.02	1.03	1.01
Tm	0.25	0.18	0.15	0.26	0.21	0.15	0.17	0.17	0.17
Yb	1.63	1.29	1.02	1.80	1.47	1.02	1.25	1.22	1.30
Lu	0.26	0.21	0.16	0.28	0.22	0.15	0.21	0.20	0.21
Ta	0.88	0.96	2.32	1.52	0.98	0.94	1.31	0.97	1.34
Sm/Nd	0.18	0.20	0.19	0.17	0.19	0.20	0.19	0.20	0.20
Eu/Eu*	0.91	0.87	1.03	0.86	0.89	1.26	0.84	0.82	0.88
ΩCe	1.00	0.96	0.99	0.98	0.98	0.97	0.89	0.98	0.88
Cr/Th	34.6	27.2	25.7	23.8	20.5	33.2	30.8	19.0	33.3
Th/Sc	0.27	0.59	0.56	0.56	0.58	0.65	0.73	0.81	0.81
Zr/Sc	5.68	8.34	12.37	10.01	8.52	12.99	11.04	11.98	18.32
LREE	1.58	1.51	1.15	2.82	1.86	1.5	0.94	1.18	0.66
HREE	1.8	1.39	1.11	1.95	1.58	1.1	1.36	1.32	1.38
MREE	1.55	1.45	1.18	2.2	1.85	1.52	0.88	1.16	0.76
MREE*	1.69	1.45	1.13	2.38	1.72	1.3	1.15	1.25	1.02

Table 3: Major and Trace Element Concentrations of Sedimentary Rocks Analyzed in this Study . D.L. : Detection Limit

Note. Uncertainties for all elements are given in the supplementary material (Table S2)

LREE = $La_{PAAS} + Pr_{PAAS} + Nd_{PAAS}$ (in ppm); MREE = $Gd_{PAAS} + Tb_{PAAS} + Dy_{PAAS}$ (in ppm);

HREE = TmPAAS + YbPAAS + LuPAAS (in ppm); MREE* = (HREE+LREE) / 2;

CIA=$[Al_2O_3/(Al_2O_3+CaO^*+Na_2O+K_2O)] \times 100$ (in molar proportions); Eu/Eu* = $Eu_N/(Sm_N \times Gd_N)^{1/2}$

where XN refers to the chondrite-normalized concentration value [Condie, 1993];

$\Omega Ce = 2 \times (Ce_{sample}/Ce_{PAAS}) / [(La_{sample}/La_{PAAS}) + (Pr_{sample}/Pr_{PAAS})]$

Sample	AR1-11E	AR1-11F	AR1-12A	AR1-14	AR1-17A	AR1-17B	AR1-20	AR1-21	AR1-23	AR1-24
Age	Cenomanian	Cenomanian	Early Turonian	Turonian	Coniacian	Coniacian	Early Santonian	Santonian?	Late Campanian	Paleocene
wt%										
SiO_2	52.29	53.10	49.47	61.86	57.11	61.77	52.75	51.21	53.19	50.80
Al_2O_3	20.00	19.04	22.95	15.43	13.45	13.13	20.50	21.98	20.75	14.83
Fe_2O_3	6.10	6.01	5.35	4.91	3.98	4.16	7.57	7.83	6.96	8.09
MnO	0.02	0.02	< D.L.	< D.L.	< D.L.	< D.L.	0.03	0.03	0.02	0.02
MgO	2.30	1.69	1.76	1.78	0.91	1.00	1.89	1.92	1.80	1.07
CaO	0.35	0.95	0.19	0.29	1.54	0.68	0.26	0.26	0.31	2.60
Na_2O	1.43	1.34	0.55	0.40	0.43	0.31	0.79	0.97	0.81	0.22
K_2O	2.98	2.68	1.62	1.36	1.17	1.05	2.36	2.95	3.19	1.50
TiO_2	1.34	1.07	0.95	0.65	0.50	0.47	1.02	1.08	0.95	0.68
P_2O_5	0.47	1.47	0.21	0.19	1.60	1.15	0.20	0.17	0.28	0.17
LOI	12.47	12.24	16.19	12.36	18.58	16.90	12.45	11.76	12.00	19.90
Total	99.75	99.60	99.22	99.23	99.26	100.62	99.80	100.16	100.26	99.87
Al/Si	0.43	0.41	0.53	0.28	0.27	0.24	0.44	0.49	0.44	0.33
CIA	76	74	89	85	74	82	83	81	80	69
ppm										
Sc	13.43	14.62	14.52	12.08	13.44	12.75	21.22	21.86	19.65	12.81
Rb	153.68	132.56	115.22	102.31	73.22	67.93	149.33	183.20	159.01	63.81
Cs	7.69	6.65	7.30	5.81	4.16	4.17	7.25	8.07	6.57	4.31
Ba	340.37	308.91	946.30	664.12	446.69	369.73	877.89	810.99	415.59	410.19
Sr	87.07	101.91	61.06	57.60	113.04	72.26	83.53	84.92	76.10	58.28
Th	14.39	16.37	9.87	7.68	9.84	9.72	17.25	21.49	19.67	13.35
U	5.49	12.01	4.35	3.30	15.54	9.38	3.97	4.44	4.86	4.27
Y	8.3	13.0	10.0	8.0	39.3	23.5	25.8	32.0	26.6	24.6
Zr	177.27	174.12	107.77	72.74	92.63	75.43	129.46	151.13	183.69	133.55
Nb	13.81	12.86	10.98	8.21	7.30	6.43	17.58	21.42	19.01	13.49
Hf	5.27	4.86	3.30	2.28	2.70	2.20	4.09	4.73	5.67	3.46
Cr	319.80	228.02	230.77	195.32	372.85	354.00	175.32	122.98	150.74	82.26
V	263.30	220.20	645.18	421.17	210.40	199.49	144.34	127.21	122.75	76.96
Co	14.68	11.18	10.03	8.88	5.16	5.12	12.10	14.05	11.89	19.01
Cu	31.50	25.16	20.33	18.32	36.12	26.80	26.05	25.31	21.44	27.25
Ni	75.29	53.16	56.40	47.64	73.86	60.67	37.91	35.60	31.67	49.59
Zn	106.40	80.21	68.22	67.48	114.85	98.88	79.63	74.47	69.55	53.10
La	12.36	22.79	19.02	16.84	38.51	26.80	54.96	68.63	54.75	47.31
Ce	21.60	49.30	32.55	31.18	61.50	46.51	107.93	138.54	109.94	96.33
Pr	2.59	6.28	3.84	3.60	7.87	5.75	12.22	15.76	12.56	11.14
Nd	9.85	23.89	13.67	13.03	29.58	21.46	44.25	57.53	45.55	40.74
Sm	1.92	4.76	2.47	2.30	5.79	4.08	7.86	10.39	8.15	7.50
Eu	0.46	1.07	0.58	0.51	1.28	0.87	1.53	1.98	1.56	1.53
Gd	1.48	3.35	1.87	1.75	5.11	3.32	6.00	7.96	6.06	5.87
Tb	0.23	0.47	0.27	0.24	0.75	0.49	0.87	1.14	0.88	0.86
Dy	1.49	2.69	1.74	1.47	4.70	3.00	5.07	6.54	5.14	4.91
Ho	0.34	0.53	0.38	0.29	1.03	0.64	1.01	1.29	1.04	0.97
Er	1.04	1.40	1.10	0.84	2.80	1.76	2.74	3.41	2.83	2.49
Tm	0.17	0.20	0.17	0.13	0.38	0.24	0.39	0.48	0.41	0.35
Yb	1.25	1.42	1.23	0.90	2.46	1.57	2.65	3.26	2.79	2.31
Lu	0.19	0.22	0.19	0.14	0.36	0.23	0.39	0.48	0.42	0.33
Ta	1.34	1.22	1.06	0.77	0.69	0.61	1.63	2.03	1.84	1.34
Sm/Nd	0.19	0.20	0.18	0.18	0.20	0.19	0.18	0.18	0.18	0.18
Eu/Eu*	0.83	0.82	0.83	0.78	0.72	0.72	0.68	0.67	0.68	0.71
ΩCe	0.92	0.99	0.92	0.96	0.85	0.90	1.00	1.01	1.01	1.01
Cr/Th	22.2	13.9	23.4	25.4	37.9	36.4	10.2	5.7	7.7	6.2
Th/Sc	1.07	1.12	0.68	0.64	0.73	0.76	0.81	0.98	1	1.04
Zr/Sc	13.2	11.91	7.42	6.02	6.89	5.92	6.1	6.91	9.35	10.43
LREE	0.92	2.05	1.36	1.26	2.82	2.02	4.2	5.38	4.28	3.77
HREE	1.32	1.52	1.3	0.96	2.66	1.71	2.83	3.48	2.99	2.47
MREE	0.95	1.93	1.15	1.02	3.13	2.03	3.56	4.66	3.6	3.48
MREE*	1.12	1.78	1.33	1.11	2.74	1.87	3.51	4.43	3.63	3.12

Table 2 (Continued)

Sample	Age	Sr (ppm)	$^{87}Sr/^{86}Sr$	± 1σ (*10^6)	Nd (ppm)	$^{143}Nd/^{144}Nd$	± 1σ	$\varepsilon_{Nd(0)}$	± 1σ	T_{DM} (Ga)
AR1-1	Early Cretaceous	206.01	0.726863	0.000005	16.46	0.512523	0.000016	-2.2	0.3	0.9
AR1-6	Late Albian	109.76	0.730869	0.000005	16.49	0.511549	0.0000047	-21.2	0.1	2.6
AR1-7	Late Albian	195.54	0.721161	0.000003	12.62	0.51167	0.000008	-18.9	0.2	2.3
AR1-8	Cenomanian	103.58	0.732824	0.000003	29.99	0.511674	0.000008	-18.8	0.2	2.1
AR1-9	Cenomanian	123.21	0.730814	0.000005	20.68	0.512608	0.000011	-0.6	0.2	0.8
AR1-10	Cenomanian	269.75	0.714598	0.000005	16.94	0.511694	0.000004	-18.4	0.1	2.3
AR1-11B	Cenomanian	82.50	0.746371	0.000006	9.08	0.511599	0.000005	-20.3	0.1	2.3
AR1-11C	Cenomanian	100.41	0.746923	0.000005	13.69	0.511581	0.000006	-20.6	0.1	2.5
AR1-11D	Cenomanian	106.65	0.722602	0.000005	6.25	0.511614	0.000009	-20.0	0.2	2.5
AR1-11E	Cenomanian	87.07	0.738315	0.000005	9.85	0.512015	0.000025	-12.2	0.5	1.8
AR1-11F	Cenomanian	101.91	0.738174	0.000004	23.89	0.511669	0.000006	-18.9	0.1	2.4
AR1-12A	Early Turonian	61.06	0.760897	0.000005	13.67	0.51178	0.00001	-16.7	0.2	2.0
AR1-14	Turonian	57.60	0.736446	0.000005	13.03	0.511634	0.000083	-19.6	1.6	2.2
AR1-17A	Coniacian	113.04	0.725604	0.000005	29.58	0.5117585	0.000011	-17.2	0.2	2.2
AR1-17B	Coniacian	72.26	0.730986	0.000005	21.46	0.511827	0.000026	-15.8	0.5	2.0
AR1-20	Late Santonian	83.53	0.753144	0.000004	44.25	0.511588	0.000006	-20.5	0.1	2.2
AR1-21	Santonian ?	84.92	0.773011	0.000006	57.53	0.511939	0.000006	-13.6	0.1	1.8
AR1-23	Late Campanian	76.10	0.774847	0.000006	45.55	0.512535	0.000008	-2.0	0.2	0.9
AR1-24	Paleocene	58.275	0.749076	0.000005	40.74	0.51159	0.000003	-20.4	0.1	2.3

Table 4: Nd–Sr isotopic systematics of sedimentary rocks analyzed in this study